Matter Distributions of Galaxy Clusters in Modified Newtonian Dynamics

Wouter Hajer

Applied Mathematics &
Applied Physics
TU Delft

Delft,
July 6, 2022
Supervisors: Dr. P. Visser
Dr. S. Eijt

Abstract

Over the past century various different discrepancies in the expected and observed behaviour of galaxies and galaxy clusters were found. Together this is called the missing mass problem and the most well known theory trying to explain these differences states that there is additional undetectable mass in the form of dark matter. Modified Newtonian Dynamics (MOND) is another theory that tries to explain these discrepancies in a different way then by introducing dark matter. Instead the theory changes Newtons law of gravity for low accelerations, smaller than Milgroms constant a_0. In this bachelor thesis we look at a discrete model to simulate MOND in galaxy clusters. To simplify calculations we will not be looking at full MOND, which holds for all accelerations but instead we look at the so called deep MOND, which only holds for accelerations much smaller than a_0.

We use two different versions of the Poisson equation, the standard version for Newtonian dynamics and a modified version for MOND, to compute the gravitational potential fields caused by a mass density distribution. This is done by using the discrete Fourier transform on an discretized region of space. The initial mass density distribution consists of a number of galaxies ranging between 50 and 1000 per cluster. Each galaxy is modelled as a sphere of constant density. To calculate the potential with MOND we use an iterative process starting from the potential we get using Newtonian dynamics. In this iterative process we made use of the Helmholtz decomposition. From the MOND potential we can compute an apparent mass distribution, which is the mass distribution that would result in the same MOND potential using Newtonian dynamics. This apparent matter distribution we use to predict at what distance of a galaxy most apparent dark matter is located. Lastly we also look at the apparent mass distributions when the galaxy cluster is projected on a 2d plane. All of these calculations were made in Python on a discrete grid of 256 $\times$ 256 $\times$ 256 points.

We looked at galaxies with a baryonic mass of $3 \cdot 10^{41}$ Kg distributed using an MOND isothermal spherically symmetric distribution function with $b = 0.4$ Mpc on a cubic region with dimensions 2 Mpc $\times$ 2 Mpc $\times$ 2 Mpc. We found for both a cluster consisting of 50 galaxies and a cluster with 1000 galaxies that the gravitational acceleration g is smaller than a_0 everywhere, so $g < a_0$ holds everywhere, but $g \ll a_0$ did not. That $g < a_0$ holds makes deep MOND a reasonable assumption, but it is not perfect everywhere. We also found that the ratio between the amount of apparent dark matter and baryonic matter, $\frac{M_{\text{Dark}}}{M_{\text{Bar}}}$, in a galaxy cluster follows a relation in the deep MOND regime of the form $\frac{M_{\text{Dark}}}{M_{\text{Bar}}} = a + \frac{b}{\sqrt{N}}$, where N is the number of galaxies in a cluster. From a least squares fit we found the following values for these variables: $a = 0.8064 \pm 0.2383$ and $b = 101.9 \pm 4.3$.

When looking at the total amount of apparent mass in concentric spheres around galaxies in our cluster we saw that this increases in three distinct phases. The middle phases, where a linear increase was seen, had a slope in the same order of magnitude as the theoretical value. We found that the average apparent mass density is the highest in the center of galaxies and decreases very quickly at higher distance to the galaxy. When the distance becomes high enough to reach neighbouring galaxies in the same cluster the average apparent mass density stabilizes and becomes almost constant, but still slightly decreases. For the projected mass density a similar pattern was found.

Contents

1. Introduction

1.1. History

At the basis of almost every new theory in physics lies an unexpected phenomenon. Often a cycle is followed where after a problem or discrepancy in our current understanding of the universe is found, several theories are formed to try to explain it. Then one or more of these theories gain popularity and experimental physicists seek for evidence to disprove or corroborate them until consensus on a certain theory is reached. To give a better understanding of the problem that the theory of Modified Newtonian Dynamics tries to solve, I will start by giving a historical overview of this cycle for this specific problem, from the first discovery of discrepancies to the current hypotheses.

1.1.1. Discovery of the problem

The first discovery of a discrepancy in the motion of galaxies was made by Fritz Zwicky [1]. In an article published in 1933 he described that the observed rotational energy of luminous matter in the coma cluster exceeded the calculated value as a result of the gravitational attraction from the baryonic matter in the cluster. With baryonic matter we mean all matter of which the particles can be directly detected instead of indirectly calculated. He first proposed the existence of a certain 'dunkle Materie' (dark matter) which could explain this discrepancy. It must be noted that what Zwicky meant with this proposition is not the same as what we understand as dark matter today [2]. Conforming to his time period, dark matter was a way of describing non-luminous objects and not directly used to describe the unknown particles which we call dark matter nowadays. Results similar to those found by Zwicky were found for different clusters of galaxies in the following years by Erik Holmberg and Sinclair Smith. Despite these results, these discrepancies did not become a popular field of study until decades later.

Near the end of the 1950's new calculations on different clusters gave similar results, which sparked new interest. In 1958, Viktor Ambartsumian proposed an explanation for the discrepancy different from the dark matter theory of Zwicky. He proposed that the observations came from the fact that galaxies and clusters of galaxies were not stable and in the process of being ripped apart. Both of these theories were supported by some and had reasons why their opponents did not like them. The theory of unstable clusters of galaxy would lead to a very short lifetime, approximately 10 to 1000 years, which would result in significantly less clusters then that were observed. On the other hand, the theory of dark matter was seen as inelegant as it would mean that all theories in astronomy were based on only a small amount of all the matter in the universe.

1.1.2. Flat rotation curves

In the years that followed new technologies, like radio astronomy and the 21-cm radio emission line, which made neutral hydrogen detectable, were developed. These led to the discovery of new evidence of the missing mass problem. Next to the mass discrepancy already found in clusters of galaxies, now similar results were found in galaxies themselves, in the form of flat rotation curves derived from the Doppler shift of the 21-cm hydrogen line. In 1970 studies about this phenomenon were published separately by both Kenneth Freeman [3] and by Vera

Rubin and Kent Ford [4]. They found that the rotational speed of solar systems at the edge of galaxies was higher then expected based on the amount of baryonic mass.

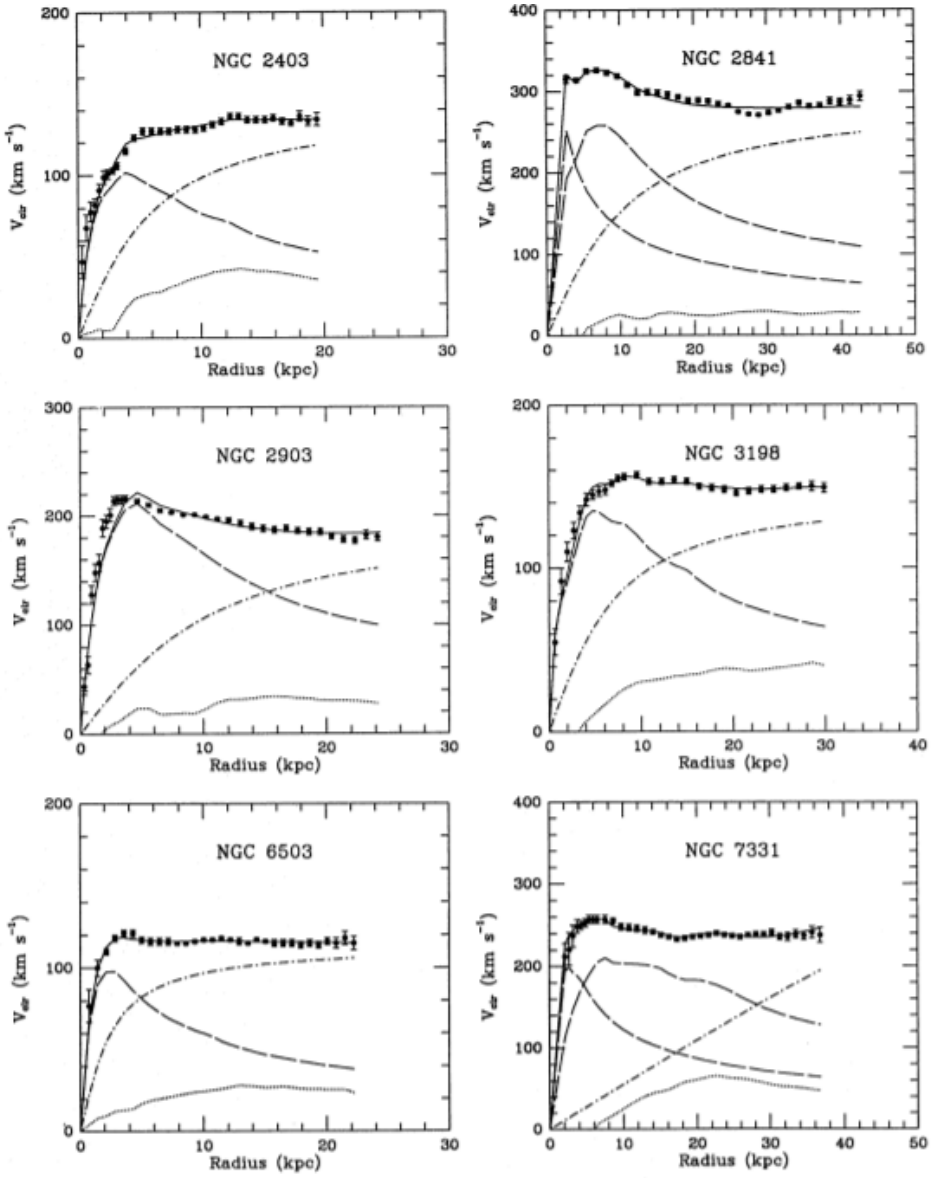

Figure 1: The rotational speed of mass in several galaxies plotted against the distance to the core of the galaxy with the best fitting models (continuous lines). Furthermore the contributions of the stellar disc (short-dashed line), the gas (long-dashed line) and the halo (dot-dashed line) are shown for each galaxy. These lines show the rotational speeds that a mass at that distance would have if only that type of mass would be present. From Sanders, Begeman and Broeils [5]

.

The calculated speed v was based on the fact that the gravitational force of all mass inside of the orbit of a solar system in a galaxy acts as the centripetal force that keeps it in orbit as written in equation (1).

$$\frac{mv^2}{r} = G\frac{mM(r)}{r^2} \tag{1}$$

Here m is the mass of the solar system, G the gravitational constant. $M(r)$ is the amount of mass located inside the orbit of the solar system, and therefore dependent on the distance to the center r. This reduces to equation (2).

$$v = \sqrt{\frac{GM(r)}{r}} \tag{2}$$

From observations of baryonic mass it was seen that after a certain radius R there was almost no new mass, so $M(r) \approx c$ for $r > R$, with c a constant. This would however mean $v(r) \sim \frac{1}{\sqrt{r}}$ for $r > R$, so it was expected that the rotational speed would drop significantly far away from the core of the galaxy, but instead the curve flattened, $v(r) \approx constant$ for $r > R$. According to equation (2) this would mean that $M(r) \sim r$ for $r > R$. While this discrepancy was described in both articles, no explanation for this phenomenon was proposed.

1.1.3. Rise in popularity of dark matter

Coinciding with the discovery of this new evidence of the missing mass problem was another search for mass. The universe can be either flat, open or closed and this relies on the amount of mass that is present in the universe. A closed universe would first expand and then slowly stop expanding and start contracting again, resulting in a collapse, while an open universe would keep expanding forever and a flat universe would slowly stop expanding and reach a constant size after some time. Which of these scenarios is true depends on the average mass density in the universe. There is a critical mass density, ρ_{crit}, and if the ratio between the mass density in the universe ρ and this ρ_{crit}, called $\Omega = \frac{\rho}{\rho_{crit}}$ is smaller than 1, the universe is open. From observations like cosmic background radiation it was calculated that the universe should be at least flat, and possibly closed, meaning $\Omega \geq 1$. However all baryonic mass in the universe amounted to values of ρ for which $\rho \ll \rho_{crit}$ and thus contradicted other observation. This let to an increased effort to find additional mass in the universe and reinforced beliefs in dark matter.

1.1.4. Modified Newtonian Dynamics

In the 1980's several other solutions were proposed that tried to solve the problem not by introducing new forms of matter, but by altering the laws of Newton under specific conditions. The mass discrepancy was observed on the scale of galaxies and clusters of galaxies, but the Newtonian dynamics held true on the scale of solar systems. As a result, many proposed solutions tried to alter the laws of Newton at big distances. With such modifications one runs into problems when looking at the resulting power in the Tully-Fisher relationship. The Tully-Fisher relationship is an observational relation between the luminosity of a galaxy L and the rotational speed of that galaxy V, first discovered by Tully and Fisher in 1977[6]. The relation is of the form $L \propto V^{\alpha}$, where α is a constant of roughly between 3.5 to 4. As for galaxies the M/L ratio is approximately constant, we get $M \propto V^{\alpha}$ [7]. Modifications of Newton laws at big distances resulted in $\alpha = 2$, which was contradicted by the experimental observation. In 1983 a solution to the missing mass problem was proposed by Mordehai Milgrom [8]. In this proposal he tried to solve the discrepancies by modifying the second law of Newton at low accelerations instead of great distances. This had many similar effects, because at big distances gravitational attractions have very low acceleration. A big difference was however that this gave a power of

$\alpha = 4$ in the Tully-Fisher relationship, confirming a lot better to the observations. This theory came to be known as Modified Newtonian Dynamics (MOND for short). The following year Milgrom worked out this theory together with Jacob Bekenstein and they proposed a slightly altered version where the Poisson equation was to be modified instead of the second law of Newton and which would reduce to the same modification under special symmetry conditions [9].

1.1.5. Newer developments in MOND

After the initial proposal of MOND by Milgrom a lot of different versions of the theories have been proposed by supporters of the theory. Some of the most famous ones are relativistic theories which reduce to MOND in the non-relativistic limit. The best known variant is probably the Tensor-Vector-Scalar (TeVeS) theory, proposed by Bekenstein in 2004 [10]. This theory still had some problems with reproducing cosmologic observations like cosmic microwave background radiation. Just recently, in 2021, Constantinos Skordis and Tom Zlosnik have proposed a modification of TeVeS which is able to reproduce these observations [11].

1.2. Gravitational lensing

An important observations that astronomers use to calculate locations of supposed dark matter on a level of a cluster are observations of gravitational lensing. Gravitational lensing is an effect that can happen when a galaxy cluster is located between an observer on Earth and another galactic object even further away then the cluster [12]. The gravitational potential field caused by the cluster can bend light coming from the galactic object and as a result distort the way in which it is observed. When strong lensing occurs it can result in distortions like multiple images of the object being visible or an Einstein ring occurring around the object. Astronomers use these gravitational lensing events as a way to observe the potential field caused by galaxy clusters and from that find a supposed matter distribution in clusters.

2. Poisson equation

2.1. Spherical coordinates

In several derivations we will use spherical coordinates. Therefore we will start this chapter with some useful definitions for spherical coordinates we will use later. We start with the basic equations for spherical coordinates. Note that we will use boldface in this document to distinguish variables that represent vectors from scalars.

$$\hat{\boldsymbol{r}} = \sin(\theta)\cos(\varphi)\hat{\boldsymbol{x}} + \sin(\theta)\sin(\varphi)\hat{\boldsymbol{y}} + \cos(\theta)\hat{\boldsymbol{z}} \tag{3}$$

$$\hat{\boldsymbol{\theta}} = \cos(\theta)\cos(\varphi)\hat{\boldsymbol{x}} + \cos(\theta)\sin(\varphi)\hat{\boldsymbol{y}} + \cos(\theta)\hat{\boldsymbol{z}} \tag{4}$$

$$\hat{\boldsymbol{\varphi}} = -\sin(\varphi)\hat{\boldsymbol{x}} + \cos(\varphi)\hat{\boldsymbol{y}} \tag{5}$$

We will also use the definition of the divergence $\nabla \cdot \boldsymbol{A}$ and the curl $\nabla \times \boldsymbol{A}$ in spherical coordinates, equations (7) and (8). Both of these can be derived from the definition of the nabla-operator ∇ in spherical coordinates for which the definition is given in equation (6).

$$\nabla = \hat{\boldsymbol{r}}\frac{d}{dr} + \hat{\boldsymbol{\theta}}\frac{1}{r}\frac{d}{d\theta} + \hat{\boldsymbol{\varphi}}\frac{1}{r\sin\theta}\frac{d}{d\varphi} \tag{6}$$

$$\nabla \cdot \boldsymbol{A} = \frac{1}{r^2}\frac{d(r^2 A_r)}{dr} + \frac{1}{r\sin\theta}\frac{d(A_\theta \sin\theta)}{d\theta} + \frac{1}{r\sin\theta}\frac{dA_\varphi}{d\varphi} \tag{7}$$

$$\begin{aligned}\nabla \times \boldsymbol{A} = {} & \frac{1}{r\sin\theta}\left(\frac{\partial}{\partial\theta}\left(A_\varphi \sin\theta\right) - \frac{\partial A_\theta}{\partial\varphi}\right)\hat{\mathbf{r}} \\ & + \frac{1}{r}\left(\frac{1}{\sin\theta}\frac{\partial A_r}{\partial\varphi} - \frac{\partial}{\partial r}\left(rA_\varphi\right)\right)\hat{\boldsymbol{\theta}} \\ & + \frac{1}{r}\left(\frac{\partial}{\partial r}\left(rA_\theta\right) - \frac{\partial A_r}{\partial\theta}\right)\hat{\boldsymbol{\varphi}}\end{aligned} \tag{8}$$

2.2. Newtonian Gravity

Before we can look at the Modified Newtonian Gravity we first need to take a closer look at standard Newtonian Gravity. This we will use to show where both theories are similar and where alterations to the theory are made. In the standard Newtonian model, gravity is an attractive force between two masses m_1 and m_2 given by equation (9).

$$\boldsymbol{F} = -G\frac{m_1 m_2}{r^2}\hat{\boldsymbol{r}} \tag{9}$$

Here $\boldsymbol{F}$ is the resulting force on m_1, G the gravitational constant, r the distance between the two objects and $\hat{\boldsymbol{r}}$ the direction vector from m_1 to m_2. If we combine this with Newton's second law (10) we will find that the acceleration caused by mass m_2 on m_1 is given by equation (11).

$$\boldsymbol{F} = \frac{d\boldsymbol{p}}{dt} = m_1\boldsymbol{a} \tag{10}$$

$$\boldsymbol{a} = -G\frac{m_2}{r^2}\hat{\boldsymbol{r}} \tag{11}$$

From this we will derive the Poisson equation. We will start by looking at a gravitational field $\boldsymbol{g_i}(\boldsymbol{r})$ at a location $\boldsymbol{r}$ caused by a point mass m at the origin. The gravitational field at the location $\boldsymbol{r}$ is just the acceleration at that specific point caused by the point mass. So we can rewrite the more general equation (11) to get equation (12) for our specific situation.

$$\boldsymbol{g}_i(\boldsymbol{r}) = -Gm\frac{\hat{\boldsymbol{r}}}{r^2} = -Gm\frac{\boldsymbol{r}}{r^3} \tag{12}$$

Now we will calculate the gravitational field as a result of n different point masses. Each point mass has a mass m_i and a location $\boldsymbol{s}_i$. We can use equation (12) to calculate the individual gravitational field $\boldsymbol{g}_i(\boldsymbol{r})$ for each mass. As gravity is a conservative force, we may use the superposition principle. So we can calculate the total gravitational field $\boldsymbol{g}(\boldsymbol{r})$ at point $\boldsymbol{r}$ by summing over the contributions $\boldsymbol{g}_i(\boldsymbol{r})$ given by every mass in the universe. So we have:

$$\boldsymbol{g}(\boldsymbol{r}) = \sum_{i=1}^{n}\boldsymbol{g_i}(\boldsymbol{r}) = -\sum_{i=1}^{n} m_i G\frac{(\boldsymbol{r}-\boldsymbol{s_i})}{|\boldsymbol{r}-\boldsymbol{s_i}|^3} \tag{13}$$

Now instead of looking at point masses we will look at the gravitational field caused by a mass density ρ. We will divide a region A into $l \times m \times n$ small cubes with equal volume $\Delta V = \Delta x \Delta y \Delta z$. We approximate the mass of each volume with $\Delta m_{ijk} \approx \Delta V \rho(\boldsymbol{s}_{ijk})$, where $\boldsymbol{s}_{ijk}$ is the center of the cube. Substituting this in equation (13) gives equation (14).

$$\boldsymbol{g}(\boldsymbol{r}) \approx -\sum_{i=1}^{l}\sum_{j=1}^{m}\sum_{k=1}^{n}\rho(\boldsymbol{s}_{ijk})\Delta V G\frac{(\boldsymbol{r}-\boldsymbol{s_{ijk}})}{|\boldsymbol{r}-\boldsymbol{s_{ijk}}|^3} \tag{14}$$

If we look at the limit were ΔV goes to zero this sum over cubes becomes a volume integral. We can thus rewrite (14) to integral form to get equation (15).

$$\boldsymbol{g}(\boldsymbol{r}) = -\int\int\int_A \rho(\boldsymbol{s})G\frac{(\boldsymbol{r}-\boldsymbol{s})}{|\boldsymbol{r}-\boldsymbol{s}|^3}dV \tag{15}$$

Now we take the divergence with respect to $\boldsymbol{r}$ on both sides. Note that our volume integral is with respect to $\boldsymbol{s}$, so we are allowed to interchange the divergence and the integral. We get:

$$\nabla\cdot\boldsymbol{g}(\boldsymbol{r}) = -\int\int\int_A \rho(\boldsymbol{s})G\left(\nabla\cdot\frac{(\boldsymbol{r}-\boldsymbol{s})}{|\boldsymbol{r}-\boldsymbol{s}|^3}\right)dV \tag{16}$$

We then use the following known theorem [13]:

$$\nabla\cdot\left(\frac{\boldsymbol{r}}{|\boldsymbol{r}|^3}\right) = 4\pi\delta(\boldsymbol{r}) \tag{17}$$

This results in:

$$\nabla\cdot\boldsymbol{g}(\boldsymbol{r}) = -4\pi G\int\rho(\boldsymbol{s})\delta(\boldsymbol{r}-\boldsymbol{s})dV \tag{18}$$

Then using the properties of the Dirac delta function this simplifies into Gauss's law for gravity, equation (19).

$$\nabla \cdot \boldsymbol{g} = -4\pi G\rho \tag{19}$$

As gravity is a conservative force, we know that $\boldsymbol{g}$ has a potential, which we will call ϕ, such that $\boldsymbol{g} = -\nabla\phi$. Writing this with $\boldsymbol{g} = -\nabla\phi$ and replacing this ∇ as shown in equation (6), we get the Poisson equation:

$$\nabla \cdot \nabla\phi = 4\pi G\rho \tag{20}$$

This equation we will use quite often.

2.3. Modified Newtonian Dynamics

Now that we have introduced the Poisson equation in standard Newtonian dynamics, we can use similar steps to find a similar equation according to Modified Newtonian Dynamics (MOND). This theory is based on the idea that Newton's second law changes when the acceleration that is caused by it is smaller than a certain acceleration constant $a_0 = 1.2 \cdot 10^{-10}$ m/s^2. When the acceleration is bigger than this constant, Newton's second law would stay the same. We can write this in formula form as equation (21).

$$\boldsymbol{F} = \begin{cases} m\,\boldsymbol{a} & \text{for} \quad a \gg a_0 \\ m\,\frac{|\boldsymbol{a}|}{a_0}\,\boldsymbol{a} & \text{for} \quad a \ll a_0 \end{cases} \tag{21}$$

This is often written with as a single equation with the interpolating function $\mu(x)$. We will define the interpolation function as in equation (22) such that we can simplify equation (21) into (23).

$$\mu(x) = \begin{cases} 1 & \text{for} \quad x \gg 1 \\ x & \text{for} \quad x \ll 1 \end{cases} \tag{22}$$

$$\boldsymbol{F} = m\,\mu\left(\frac{|\boldsymbol{a}|}{a_0}\right)\boldsymbol{a} \tag{23}$$

For μ various different functions have been proposed. Here I will show two of the possibilities, the so called simple interpolating function in equation (24) and the standard interpolating function in equation (25)[14][8].

$$\mu(x) = \frac{x}{1+x} \tag{24}$$

$$\mu(x) = \frac{x}{\sqrt{1+x^2}} \tag{25}$$

Now we will take a closer look at the impact of changing Newton's second law for small accelerations. We will thus be looking just at the domain were $a \ll a_0$, as everything stays the same in the other domain. This domain is called the deep MOND domain and therefore we will specify equations on that domain with the subscript DM. If we follow what we did for Newtonian gravity and equate the deep MOND part of equation (23) to the force of gravity (9), we get the following equation for the acceleration as a result of a point mass at the origin. Here we will call the acceleration again $\boldsymbol{g}$, to specify we are looking at the gravitational acceleration.

$$\frac{|\boldsymbol{g}_{\text{DM}}|}{a_0}\boldsymbol{g}_{\text{DM}} = -G\frac{m_2}{r^2}\hat{\boldsymbol{r}} \tag{26}$$

If we now take the absolute value of both sides of this equation we can simplify it into equation (27).

$$|\boldsymbol{g}_{\text{DM}}| = \frac{\sqrt{Gm_2a_0}}{r} \tag{27}$$

From this we can make the important observation that the acceleration caused by gravity in the deep MOND case relates to distance with $|\boldsymbol{g}_{\text{DM}}| \propto \frac{1}{r}$ as opposed to $|\boldsymbol{g}| \propto \frac{1}{r^2}$ in the standard Newtonian case.

If we now take the same steps on the right hand side of equation (26) as we did in the Newtonian case to get to the Poisson equation, we get equation (28) in the deep MOND case.

$$\nabla \cdot \left(\frac{|\boldsymbol{g}_{\text{DM}}|}{a_0}\, \boldsymbol{g}_{\text{DM}} \right) = -4\pi G\rho \tag{28}$$

In this case it is slightly more difficult to show that $\boldsymbol{g}_{\text{DM}}$ has a potential, as it is no longer directly proportional to the gravitational force. However, we still have that the gravitational acceleration of a point mass in the origin has only a factor in the $\hat{\boldsymbol{r}}$ direction and this term is only dependent on $\boldsymbol{r}$. So we have in that case $\nabla \times \boldsymbol{g}_{i,\text{DM}} = 0$. But then, as the mass density field can be seen as infinitely many point masses each giving a small conservative acceleration, we have that the sum is also conservative, $\nabla \times \boldsymbol{g}_{\text{DM}} = 0$. So we once more have a potential defined as $\boldsymbol{g}_{\text{DM}} = -\nabla\phi_{\text{DM}}$. Thus we can make an equation for MOND that is analogous to the Poisson equation.

$$\nabla \cdot \left(\frac{|\nabla\phi_{\text{DM}}|}{a_0}\nabla\phi_{\text{DM}} \right) = 4\pi G\rho \tag{29}$$

If we combine the two cases into one formula again this gives us one generic function for the Poisson equation with the interpolation function, equation (30).

$$\nabla \cdot \left(\mu\left(\frac{|\nabla\phi|}{a_0} \right) \nabla\phi \right) = 4\pi G\rho \tag{30}$$

3. Distributions of galaxies in a cluster

To make a model for the effects of both Newtonian gravity and MOND in a galaxy cluster we start with a mass distribution. We will do this by defining a relation between the mass density ρ and the distance to the center of the galaxy cluster r. Then we will use that equation to get to a distribution function, such that in the limit with infinite galaxies the mass is distributed uniformly with a density $\rho(r)$. To get to this relation between ρ and r we make two assumptions.

The first assumption is that ϕ in the Poisson equation is spherically symmetric. Using this assumption we can simplify the Poisson equation in spherical coordinates to a differential equation between ϕ and ρ. This can be done for both the standard Newtonian Poisson equation and the corresponding equation for deep MOND, resulting in different equations. We will look at both of these cases and at the differences that the resulting distributions functions give.

The second assumption we make is that the temperature in the galaxy cluster is constant, giving an isothermal distribution function. Using this we can derive a second relation between ϕ and ρ from the ideal gas law and the hydrostatic equilibrium. For this we will look at galaxies in a cluster as if they are particles in a gas.

3.1. Newtonian Gravity

We will start by looking at the effects of a spherically symmetrical gravitational potential on the Poisson equation (31), which we previously derived as equation (20).

$$\nabla \cdot \nabla \phi = 4\pi G\rho \tag{31}$$

Now we assume that ϕ is spherically symmetrical and therefore, using the definition of ∇ as stated in equation (6) we get equation (32).

$$4\pi G\rho = \nabla \cdot \left(\hat{r}\frac{d\phi}{dr} + \hat{\theta}\frac{1}{r}\frac{d\phi}{d\theta} + \hat{\varphi}\frac{1}{r\sin\theta}\frac{d\phi}{d\varphi} \right) = \nabla \cdot \hat{r}\frac{d\phi}{dr} \tag{32}$$

Now using equation (7) with $A = \hat{r}\frac{d\phi}{dr}$ we can rewrite this even further. As $A_\theta = A_\varphi = 0$ we get equation (33).

$$\frac{1}{r^2}\frac{d\left(r^2\frac{d\phi}{dr}\right)}{dr} = 4\pi G\rho \tag{33}$$

This is the first relation between the potential ϕ and the density ρ we will use in the derivation of the distribution function with Newtonian gravity further on.

3.2. Modified Newtonian Gravity

We will now take the same steps we did for Newtonian gravity for the modified Poisson equation for deep MOND, equation (34), which we previously derived as equation (29).

$$\nabla \cdot \left(\frac{|\nabla \phi_{\text{DM}}|}{a_0} \nabla \phi_{\text{DM}} \right) = 4\pi G\rho \tag{34}$$

We will rewrite this equation using spherical coordinates. We start by looking at the left hand side of equation (34) and rewriting it using the definition of ∇ as stated in equation (6). This gives:

$$\nabla \cdot \left(\frac{1}{a_0} \left| \hat{r} \frac{d\phi}{dr} + \frac{\hat{\theta}}{r} \frac{d\phi}{d\theta} + \frac{\hat{\varphi}}{r \sin(\theta)} \frac{d\phi}{d\varphi} \right| \left(\hat{r} \frac{d\phi}{dr} + \frac{\hat{\theta}}{r} \frac{d\phi}{d\theta} + \frac{\hat{\varphi}}{r \sin(\theta)} \frac{d\phi}{d\varphi} \right) \right) \tag{35}$$

As we assume that the mass is distributed homogeneous in the θ and φ directions, the derivatives of ϕ with respect to those directions becomes zero. Furthermore we have that $\left|\hat{r}\frac{d\phi}{dr}\right| = \left|\frac{d\phi}{dr}\right|$, meaning we can simplify equation (35) into equation (36).

$$\nabla \cdot \left(\frac{1}{a_0} \left| \frac{d\phi}{dr} \right| \left(\hat{r} \frac{d\phi}{dr} \right) \right) \tag{36}$$

Now for the divergence we can once more use equation (7) with now $A = \frac{1}{a_0}\left|\frac{d\phi}{dr}\right|\frac{d\phi}{dr}\hat{r}$. As we again have $A_\theta = A_\varphi = 0$, we now get equation (37) for the left hand side of equation (34).

$$\frac{1}{a_0 r^2} \frac{d\left(r^2 \left|\frac{d\phi}{dr}\right| \frac{d\phi}{dr}\right)}{dr} \tag{37}$$

Lastly we can use the assumption that for gravity the potential always increases if your distance to the mass increases, so $\frac{d\phi}{dr} > 0$. Combining this all, we now have that, using the assumption of spherical symmetric potentials, equation (34) has become equation (38).

$$\frac{1}{a_0 r^2} \frac{d\left(r^2 \left(\frac{d\phi}{dr}\right)^2\right)}{dr} = 4\pi G\rho \tag{38}$$

3.3. State in Thermodynamic Equilibrium

The second equation we will use for both distributions is derived from a substitution between the ideal gas law (39) and the hydrostatic equilibrium (40). In an ideal theoretical galaxy cluster both of these equations have to be satisfied.

$$p = nk_B T \tag{39}$$

$$\nabla p = -mn\nabla\phi \tag{40}$$

In these equations n represents the number of particles per volume unit, which in our case corresponds with the number of galaxies in the cluster divided by the volume of the cluster. Furthermore, p is the pressure, m is the mass of one galaxy and k_B is the Boltzmann constant. The temperature T can be calculated with $\frac{3}{2}k_B T = \frac{1}{2}mv_0^2$, with v_0 the average speed of a galaxy in the cluster. Substituting equation (39) into equation (40) gives equation (41). As we assume that the galaxy cluster is isothermal, T is constant and can therefore be put in front of the ∇-operator.

$$k_B T \nabla n = -mn\nabla\phi \tag{41}$$

This we can simplify even further using our assumption that the galaxies in a cluster are distributed spherically symmetric. This gives that $\nabla n = \hat{r}\frac{dn}{dr}$ and $\nabla\phi = \hat{r}\frac{d\phi}{dr}$. Furthermore we have that by the chain rule $\frac{dn}{d\phi} = \frac{dn}{dr}\frac{dr}{d\phi}$, so $\frac{\nabla n}{\nabla\phi} = \frac{dn}{dr}\frac{dr}{d\phi} = \frac{dn}{d\phi}$. Thus we can rewrite equation (41) into equation (42).

$$\frac{dn}{n} = \frac{-m}{k_B T} d\phi \tag{42}$$

Integrating both sides of equation (42) gives the following result:

$$\log\left(\frac{n}{c_1}\right) = \frac{-m}{k_B T}\phi \tag{43}$$

We get c_1 as an integration constant with unit m^{-3}. Now taking the exponent of both sides of this equation results in the following equation:

$$n = c_1 e^{\frac{-m\phi}{k_B T}} \tag{44}$$

Here we work with galaxies represented as spherical masses, so we have $\rho = mn$ and thus we can rewrite this into:

$$\rho = c_2 e^{\frac{-m\phi}{k_B T}} \tag{45}$$

We have $c_2 = mc_1$. c_2 has as unit $\mathrm{kg\,m}^{-3}$. An interesting observation we can make is that the term $\frac{-m\phi}{k_B T}$ in the exponent equals the Boltzmann factor.

3.4. Isothermal Distribution functions

Using the results of the previous paragraphs we can find a distribution function that is both spherically symmetric and isothermal. To do this the distribution function must adhere to both the thermodynamic equation (45) and either the spherically symmetric Poisson equation (33) or the spherically symmetric MOND Poisson equation (38). From this we can derive two different distribution functions which we will call the Newtonian isothermal distribution and the deep MOND isothermal distribution. We will start by deriving the Newtonian isothermal distribution function.

3.4.1. Newtonian isothermal distribution

The Newtonian isothermal distribution function must thus satisfy the following two equations, which are the thermodynamic equation (45) and the spherically symmetric Poisson equation (33) restated.

$$\frac{1}{r^2}\frac{d\left(r^2 \frac{d\phi}{dr}\right)}{dr} = 4\pi G\rho \tag{46}$$

$$\rho = c_2 e^{\frac{-m\phi}{k_B T}} \tag{47}$$

Using these two equations relating the potential to the mass density we can now derive formulas for both $\phi(r)$ and $\rho(r)$ by proposing a solution for ϕ and showing that it satisfies these equations. As the resulting potential we propose:

$$\phi = c\log(r) \tag{48}$$

Here c is a constant. If we substitute this into equation (46) we get equation (49)

$$4\pi G\rho = \frac{1}{r^2}\frac{d\left(r^2\frac{d(c\log(r)}{dr}\right)}{dr} = \frac{1}{r^2}\frac{dcr}{dr} = \frac{c}{r^2} \tag{49}$$

This we can also rewrite as equation (50).

$$\rho = \frac{c}{4\pi G r^2} \tag{50}$$

If we now substitute our proposal for ϕ in equation (47) we get the following equation:

$$\rho = c_2 e^{\frac{-mc\log(r)}{k_B T}} = c_2 r^{\frac{-mc}{k_B T}} \tag{51}$$

So to make sure both equation (50) and equation (51) are the same, we must have that $c = \frac{2k_B T}{m}$ and $c_2 = \frac{c}{4\pi G} = \frac{k_B T}{2\pi G m}$. Thus this results in the following equations for ϕ, equation (52), and ρ, equation (53).

$$\phi(r) = \frac{2k_B T}{m}\log(r) \tag{52}$$

$$\rho(r) = \frac{k_B T}{2\pi G m r^2} \tag{53}$$

The relation between ρ and r we have found we will use in the model as a way of distributing the galaxies in our galaxy cluster.

3.4.2. Deep MOND isothermal distribution

We can now follow similar steps to find a distribution function using the spherically symmetrical deep MOND modified Poisson equation instead. The deep MOND isothermal distribution function must thus satisfy the following two equations, the spherically symmetric deep MOND modified Poisson equation (38) and the thermodynamic equation (45), restated here as respectively equation (54) and equation (55).

$$\frac{1}{a_0 r^2}\frac{d\left(r^2\left(\frac{d\phi}{dr}\right)^2\right)}{dr} = 4\pi G\rho \tag{54}$$

$$\rho = c_2 e^{\frac{-m\phi}{k_B T}} \tag{55}$$

We now propose a different function for ϕ as a solution to this set of equations. This function will contain two constants, b and c. We will find that we can introduce b as a constant with unit m that describes at what radius there is the greatest amount of mass and it can be chosen to generate different sizes of galaxy clusters. The value for c will once more follow from the substitution.

$$\phi = c\log\left(1 + \frac{r^{3/2}}{b^{3/2}}\right) \tag{56}$$

We will substitute this into the first two equations above and show that it is indeed a solution. This will also give us a solution for ρ. To do this without cluttering the equations to much, we will first show the following derivatives of ϕ:

$$\frac{d\phi}{dr} = c\frac{3}{2}\frac{r^{1/2}}{b^{3/2}+r^{3/2}} \tag{57}$$

$$r^2\left(\frac{d\phi}{dr}\right)^2 = c^2\frac{9}{4}\frac{r^3}{\left(b^{3/2}+r^{3/2}\right)^2} \tag{58}$$

$$\frac{d\left(c^2\frac{9}{4}\frac{r^3}{\left(b^{3/2}+r^{3/2}\right)^2}\right)}{dr} = \left(c^2\frac{27}{4}\frac{b^{3/2}r^2}{\left(r^{3/2}+b^{3/2}\right)^3}\right) \tag{59}$$

If we combine all of these derivatives and our candidate solution for ϕ into equation (54) we get the following equation:

$$4\pi G a_0\rho = \frac{1}{r^2}\frac{d\left(r^2\left(\frac{d\phi}{dr}\right)^2\right)}{dr} = \frac{1}{r^2}\left(c^2\frac{27}{4}\frac{b^{3/2}r^2}{\left(r^{3/2}+b^{3/2}\right)^3}\right) = c^2\frac{27}{4}\frac{b^{3/2}}{\left(r^{3/2}+b^{3/2}\right)^3} \tag{60}$$

By rewriting this our first equation for ρ becomes equation (61).

$$\rho = \frac{c^2}{\pi G a_0 b^3}\frac{27}{16}\frac{b^{9/2}}{\left(r^{3/2}+b^{3/2}\right)^3} = \frac{c^2}{\pi G a_0 b^3}\frac{27}{16}\left(1+\frac{r^{3/2}}{b^{3/2}}\right)^{-3} \tag{61}$$

The second equation for ρ comes from substituting our proposed solution for ϕ into the thermodynamic equation (55). We get equation (62) as a solution for ρ.

$$\rho = c_2 e^{\frac{-mc\log\left(1+\frac{r^{3/2}}{b^{3/2}}\right)}{k_B T}} = c_2\left(1+\frac{r^{3/2}}{b^{3/2}}\right)^{\frac{-mc}{k_B T}} \tag{62}$$

We can now use that both of these functions for ρ must be the same to find the values of the used constant. We have that $c_2 = \frac{c^2}{\pi G a_0 b^3}\frac{27}{16}$ and that $-3 = \frac{-mc}{k_B T}$, which can be rewritten as $c = \frac{3k_B T}{m}$. So our final solutions for ϕ and ρ which satisfy equations (54) and (55) are respectively equation (63) and equation (64).

$$\phi(r) = \frac{3k_B T}{m}\log\left(1+\frac{r^{3/2}}{b^{3/2}}\right) \tag{63}$$

$$\rho(r) = \frac{k_B^2 T^2}{m^2\pi G a_0 b^3}\frac{243}{16}\left(1+\frac{r^{3/2}}{b^{3/2}}\right)^{-3} \tag{64}$$

4. Model

4.1. Used constants

In the model we use a variety of parameters and constants. In the first table below all constants are listed. In the second table the values of chosen parameters are listed. The baryonic mass and radius of a galaxy are modelled by the values of the Milky Way.

Abbreviation	Name	Value
G	Gravitational constant	$6.6743 \cdot 10^{-11}\ \mathrm{m^3\,kg^{-1}\,s^{-2}}$
M_{Sol}	Solar mass	$1.9885 \cdot 10^{30}\ \mathrm{Kg}$
k_{B}	Boltzmann constant	$1.3806 \cdot 10^{-23}\ \mathrm{m^2\,Kg\,s^{-2}\,K^{-1}}$
Mpc	Megaparsec	$3.0857 \cdot 10^{22}\ \mathrm{m}$
a_0	Milgroms constant	$1.2 \cdot 10^{-10}\ \mathrm{m\,s^{-2}}$

Abbreviation	Name	Value
r_{C}	Cluster radius	1 Mpc
r_{G}	Galaxy radius	0.03 Mpc
M_{G}	Baryonic galaxy mass	$1.5 \cdot 10^{11} M_{\mathrm{Sol}}$
b	Distance parameter	0.4 Mpc
n_{steps}	Number of steps	256

4.2. Placing a galaxy cluster

We model our galaxy clusters using mass density functions derived in the previous chapter. We will integrate this function to get a cumulative mass function $M(r)$ dependent on the radius where M describes the mass inside a radius r from the origin of the cluster. Then we will invert this function to get a function that gives the radius $r(M)$ that contains a certain amount of mass. Lastly we will convert this function by normalization into a distribution function $R(f)$ that gives a radius for a number f, chosen by a uniform distribution function between 0 and 1. We will do this for both mass density functions we previously derived.

4.2.1. The Newtonian case

In the Newtonian case we had derived the following isothermal spherically symmetric mass density function, equation (53), which we have restated in equation (65).

$$\rho(r) = \frac{k_B T}{2\pi G m r^2} \tag{65}$$

Integrating the mass density over the total volume gives the total amount of mass in the cluster Nm, where N is the number of galaxies in the cluster and m is the mass of a single galaxy. We have:

$$\begin{aligned} Nm &= \int\int\int \rho(x,y,z)dV \\ &= 4\pi \int_0^\infty \rho(r)r^2 dr \\ &= 4\pi \int_0^\infty \frac{k_B T}{2\pi G m r^2} r^2 dr \\ &= 4\pi \int_0^\infty \frac{k_B T}{2\pi G m} dr \end{aligned} \tag{66}$$

We can easily see that for each interval of r the same amount of mass is present and thus the total amount of mass goes to infinity if r goes to infinity. To make our mass density normalizable we will introduce a new constant d, which represents the outer extent of our galaxy cluster. Then our Newtonian mass distribution is changed to equation (67), which is normalizable.

$$\rho(r) = \begin{cases} \frac{k_B T}{2\pi G m r^2} & \text{for} \quad r \leq d \\ 0 & \text{for} \quad r > d \end{cases} \tag{67}$$

Now we once more try to find the total mass by integrating this over the total volume. We find:

$$Nm = 4\pi \int_0^d \frac{k_B T}{2\pi G m} dr = \frac{2k_B T}{Gm} d \tag{68}$$

We thus have that the number of galaxies is correlated with the temperature in the galaxy cluster by $N = \frac{2k_B T d}{G m^2}$. We can therefore simplify our mass density into equation (69).

$$\rho(r) = \begin{cases} \frac{Nm}{4\pi r^2 d} & \text{for} \quad r \leq d \\ 0 & \text{for} \quad r > d \end{cases} \tag{69}$$

Then the cumulative mass $M(r)$ contained in a sphere with radius r is given by:

$$M(r) = 4\pi \int_0^r \rho(r) r^2 dr = \begin{cases} \frac{Nmr}{d} & \text{for} \quad r \leq d \\ Nm & \text{for} \quad r > d \end{cases} \tag{70}$$

Dividing by the total mass in the galaxy cluster gives us the cumulative distribution function, equation (71).

$$F(r) = \begin{cases} \frac{r}{d} & \text{for} \quad r \leq d \\ 1 & \text{for} \quad r > d \end{cases} \tag{71}$$

If we invert this on the region $r \leq d$ it gives (72). This formula we will use to determine the distance of a galaxy to the center of our cluster, with f a number between 0 and 1 chosen by a uniform distribution.

$$R(f) = df \tag{72}$$

In figure 2 you can see how galaxies are distributed for a random realization by this function. The histogram represents the distance of 10000 galaxies to the center. The x-axis is given in units of d, where the distribution is constant until a distance d and 0 afterwards. Furthermore a line is plotted showing the theoretical value of the mass distribution. This is obtained by

integrating $\rho(r)$ in the θ and φ directions and equals $\frac{1}{d}$. If integrated in the r direction, this function equals 1. The sum of the height times the width of each bin in the histogram also equals 1.

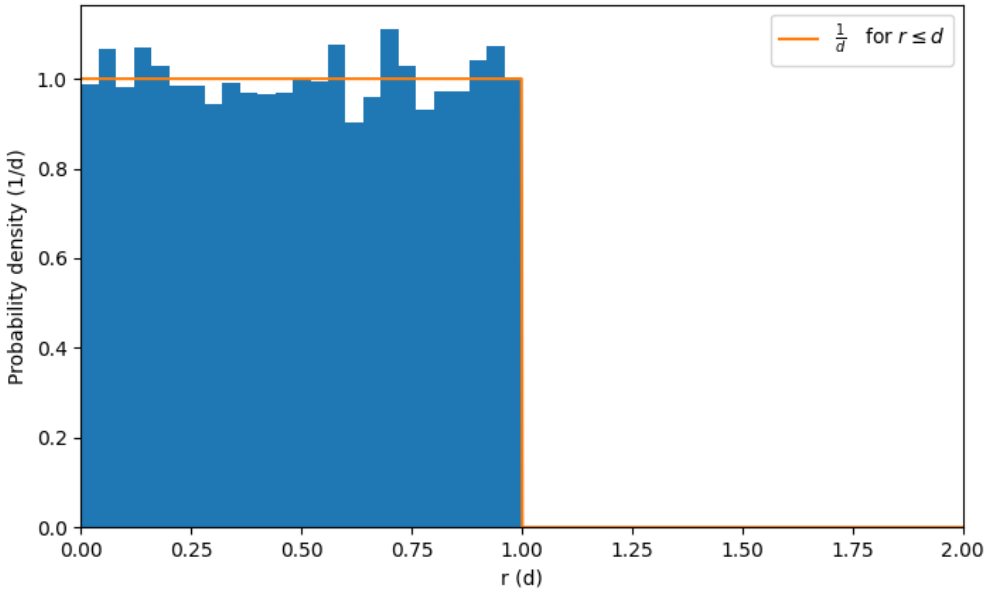

Figure 2: Histogram of how galaxies are distributed in the r-direction under an isothermal distribution in a galaxy cluster. This histogram is the result of one random realization of the distribution function with 10000 galaxies. There is also an orange curve plotted representing the theoretical distribution, which is the mass density function $\rho(r)$ integrated in the φ and θ directions and divided by the total mass. d is a constant we may freely choose and is also the cutoff point of our distribution.

4.2.2. The MOND case

Recall the isothermal spherically symmetric mass density function we found for a galaxy cluster with deep MOND in the previous chapter, equation (73).

$$\rho(r) = \frac{k_B^2 T^2}{m^2 \pi G a_0 b^3} \frac{243}{16} \left(1 + \frac{r^{3/2}}{b^{3/2}}\right)^{-3} \tag{73}$$

This we will simplify for easier reading to equation (74).

$$\rho(r) = \rho_0 \left(\frac{r^{3/2}}{b^{3/2}} + 1\right)^{-3} \tag{74}$$

Here we define that $\rho_0 = \rho(0) = \frac{k_B^2 T^2}{m^2 \pi G a_0 b^3} \frac{243}{16}$.

The total mass in a cluster defined by the mass distribution in equation (74) can be found by integrating it over the total volume. Thus we have that:

$$\begin{aligned} Nm &= \int\int\int \rho(x,y,z)dV \\ &= 4\pi \int_0^\infty \rho(r) r^2 dr \\ &= 4\pi\rho_0 \int_0^\infty \left(\frac{r^{3/2}}{b^{3/2}} + 1\right)^{-3} r^2 dr \\ &= 4\pi\rho_0 b^3 \int_0^\infty \left(\frac{r^{3/2}}{b^{3/2}} + 1\right)^{-3} \frac{r^2}{b^2} d\frac{r}{b} \\ &= 4\pi\rho_0 b^3 \int_0^\infty \left(x^{3/2} + 1\right)^{-3} x^2 dx \\ &= \frac{4\pi}{3} b^3 \rho_0 \end{aligned} \tag{75}$$

Here we have substituted $x = \frac{r}{b}$. This is quite an interesting result as the total mass of our galaxy cluster equals the mass in a sphere with radius b and mass density ρ_0. Furthermore it gives that $\rho_0 = \frac{3Nm}{4\pi b^3}$, which also means that the number of galaxies in our cluster is directly related to the isothermal temperature in our cluster and therefore the speed of the galaxies inside the cluster.

Now we will find a cumulative distribution function of the mass in our universe and by inverting it make a formula for distributing the galaxies in our model. We start by calculating the total mass in a sphere with radius r, using the same steps as in equation (75), but now integrating to r instead of ∞. Also using our new definition of ρ_0 this gives equation (76).

$$M(r) = Nm \frac{\frac{r^3}{b^3}}{\left(\frac{r^{3/2}}{b^{3/2}} + 1\right)^2} = Nm \frac{r^3}{\left(r^{3/2} + b^{3/2}\right)^2} \tag{76}$$

Dividing by the total mass in the galaxy cluster this gives us the cumulative distribution function, equation (77).

$$F(r) = \frac{r^3}{(r^{3/2} + b^{3/2})^2} \tag{77}$$

If we invert this it gives (78). This formula we will use to determine the distance of a galaxy to the center of our cluster, with f a number between 0 and 1 chosen by a uniform distribution.

$$R(f) = \sqrt[3]{\frac{b^3(f^2 + 2f^{3/2} + f)}{(f-1)^2}} \tag{78}$$

In figure 3 you can see how galaxies are distributed by this function. The histogram represents the distance of 10000 galaxies to the center. The x-axis is expressed in terms of b, where the distribution peaks at $b = 1$. Furthermore, a line is plotted showing the theoretical distribution given by $\frac{3}{b^3}\frac{r^2}{\left(\frac{r^{3/2}}{b^{3/2}}+1\right)^3}$, which is $\rho(r)$ integrated in the θ and φ directions. If integrated in the r direction, this function equals 1. The sum of the height times the width of each bin in the histogram also equals 1.

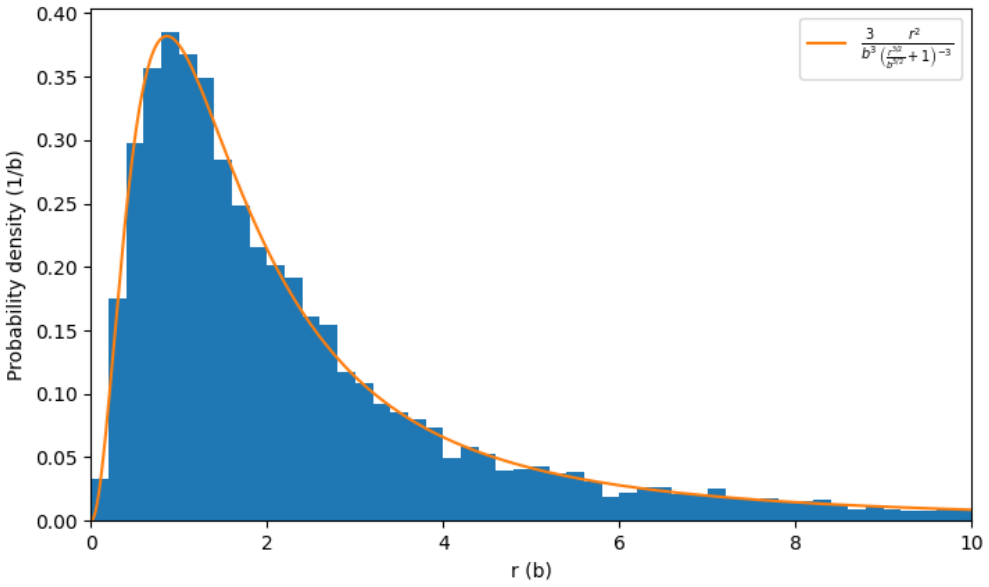

Figure 3: Histogram of the way galaxies are distributed in our model in the r-direction under a modified isothermal distribution using the MOND-Poisson equation, from equation (78). There is also an orange curve plotted representing the theoretical distribution, which is the mass density function $\rho(r)$ integrated in the φ and θ directions and divided by the total mass. b is a constant we may freely choose, the function peaks at $b = 1$.

In the simulation we will use this distribution function to distribute galaxies in modelled clusters. The reason why we take the MOND version over the Newtonian version is that fact that an arbitrary cutoff is not necessary. This makes the distribution of galaxies more dynamic. We have chosen to take $b = 0.4$ Mpc, as this leads to a large number of galaxies being located near the center of the region we simulate while still having a some galaxies near the edges.

4.3. The Fourier transform

In our model we will calculate gravitational fields as a result of galaxies in a cluster from the Poisson equation and its MOND equivalent. To do this in a computationally easy way we do a lot of calculations in the Fourier Domain. Before going further into this we will first recap the basic definition of the Fourier transform, show one of its properties that helps us with the Poisson equation and then show the definition of the Fast Fourier Transform.

The 3-dimensional Fourier transform of a function $f(\boldsymbol{x})$ and its inverse are defined by the following two equations, (79) and (80).

$$\mathcal{F}\{f\}(\boldsymbol{k}) = \tilde{f}(\boldsymbol{k}) = (2\pi)^{-3/2} \int_{-\infty}^{\infty}\int_{-\infty}^{\infty}\int_{-\infty}^{\infty} f(\boldsymbol{x}) e^{-i\boldsymbol{k}\cdot\boldsymbol{x}} d\boldsymbol{x} \tag{79}$$

$$\mathcal{F}^{-1}\{\tilde{f}\}(\boldsymbol{x}) = f(\boldsymbol{x}) = (2\pi)^{-3/2} \int_{-\infty}^{\infty}\int_{-\infty}^{\infty}\int_{-\infty}^{\infty} \tilde{f}(\boldsymbol{x}) e^{i\boldsymbol{k}\cdot\boldsymbol{x}} d\boldsymbol{k} \tag{80}$$

For the 3-dimensional Fourier transform the following differentiation identity holds:

$$\mathcal{F}\{\nabla f\} = i\boldsymbol{k}\tilde{f} \tag{81}$$

and we thus get equation (82) by doing this twice, which we can use on the left hand side of the Poisson equation.

$$\mathcal{F}\{\nabla^2 \phi\} = -\boldsymbol{k}^2 \tilde{\phi} \tag{82}$$

Recall the Poisson equation for gravity in the Newtonian case, previously stated in equation (20).

$$\nabla^2 \phi = 4\pi G\rho \tag{83}$$

We can now linearise this equation by taking the Fourier transform of both sides and using the property we just showed, which gives equation (84).

$$\boldsymbol{k}^2 \tilde{\phi} = -4\pi G\tilde{\rho} \tag{84}$$

Here $\tilde{\phi}$ and $\tilde{\rho}$ are the Fourier transforms of respectively ϕ and ρ. Furthermore we have that $\boldsymbol{k}^2$ is the square of the two norm of the location vector in Fourier space. In the 3D case we have $\boldsymbol{k}^2 = k_x^2 + k_y^2 + k_z^2$. So now we have a direct equation to find the Fourier transformed potential from the Fourier transform of the mass distribution without derivatives. This function we will use in our Python model to make the calculations faster.

4.4. Discrete and Fast Fourier Transform

In our model we make discrete calculations, so we will work with the discrete Fourier transform (DFT) instead of the regular Fourier transform. As the DFT has similar properties as the Fourier transform, we can still use our simplified Poisson equation in the Fourier domain. To further lower the computational load of our model we will also use the Fast Fourier Transform (FFT) to calculate the DFT in our model. We will now first show the definition of the DFT and then explain why we will use the FFT to calculate this efficiently.

The 3-dimensional discrete Fourier transform of an array $x_{\boldsymbol{n}}$ and its inverse are defined by the following two equations, (85) and (86).

$$\mathcal{F}\{x_{\boldsymbol{n}}\} = X_{\boldsymbol{k}} = \sum_{\boldsymbol{n}=0}^{\boldsymbol{N}-1} x_{\boldsymbol{n}} e^{-i2\pi \boldsymbol{k}\cdot(\boldsymbol{n}/N)} \tag{85}$$

$$\mathcal{F}^{-1}\{X_{\boldsymbol{k}}\} = x_{\boldsymbol{n}} = \frac{1}{N^3} \sum_{\boldsymbol{n}=0}^{\boldsymbol{N}-1} x_{\boldsymbol{n}} e^{i2\pi \boldsymbol{n}\cdot(\boldsymbol{k}/N)} \tag{86}$$

Here $\boldsymbol{N}$ is the number of elements in the array in each direction, so in our case $\boldsymbol{N} = (N, N, N)$ as the array has the same length in each direction. The sum $\sum_{\boldsymbol{n}=0}^{\boldsymbol{N}-1}$ is just a sum over all elements in the array, written in vector notation.

We will use the DFT on a finite region. The DFT will act as if the values given to it are periodic in all directions. As this periodicity is artificial this will result in strange and incorrect values at the edges of our region. Because of this we will calculate the DFT on a larger region and only use the middle half in each direction for our results.

The fast Fourier transform is not once more a different version of the Fourier transform. Instead it is a way to compute the DFT quicker. The complexity of computing a DFT normally is $\mathcal{O}(N^2)$ and the FFT reduces this to $\mathcal{O}(N \log N)$. This is done by using a different order for computing the steps of the sum in the DFT instead the just going through the values of $\boldsymbol{N}$ from small to large. Using this different algorithm calculations that otherwise had to be done several times have to be done only once, saving computing time.

4.5. Fourier transform of the Newtonian Poisson equation

To illustrate the method of calculating the potential field from a discrete mass distribution using the FFT in Python we will show a simple example. This example we will also use to compare the results of our discrete calculations and the corresponding analytical values. We calculate the gravitational field of two silicon spheres with a mass M of 100 kg and a distance of 1 m between their centers of mass in the z direction. As silicon has a density ρ of 2329 kg/m^3, this means the spheres have a radius of $r = \sqrt[3]{\frac{3V}{4\pi}} = \sqrt[3]{\frac{3M}{4\pi\rho}} = 0.217$ m.

To do this we first discretize a volume around these spheres with as origin the center of mass of the system. As we do this with 256 steps in the x, y and z direction we get an 3d array with 2^{24} points, all representing small volumes. We the let the mass density ρ of each volume be determined by the mass density at the center of the volume, giving us a vector representation for ρ. In this specific example the mass density is either the mass density of silicon, inside the spheres, or 0. Using the FFT we can now get the Fourier transform $\tilde{\rho}$ of this array and then calculate the corresponding Fourier transform $\tilde{\phi}$ of the potential field with equation (84). Here we use the discretized k vectors and it is important to note that at the origin we have $\boldsymbol{k}^2 = 0$. This means we cannot divide by this without altering $\boldsymbol{k}^2$. To circumvent this problem we define the inverse of $\boldsymbol{k}^2$ to be 0 at the origin:

$$\frac{1}{\boldsymbol{k}^2(0,0,0)} = 0 \tag{87}$$

Note that this only affects our value for $\tilde{\phi}$ at the origin. A different value at the origin in Fourier domain corresponds to a constant increase everywhere in the real domain. More specifically, a

function with the value 0 at the origin in the Fourier domain has an average value of 0. As it is a potential, this does not matter for our solution as we may choose to add a constant everywhere in the potential. Finally we can use the inverse FFT to get a potential field ϕ.

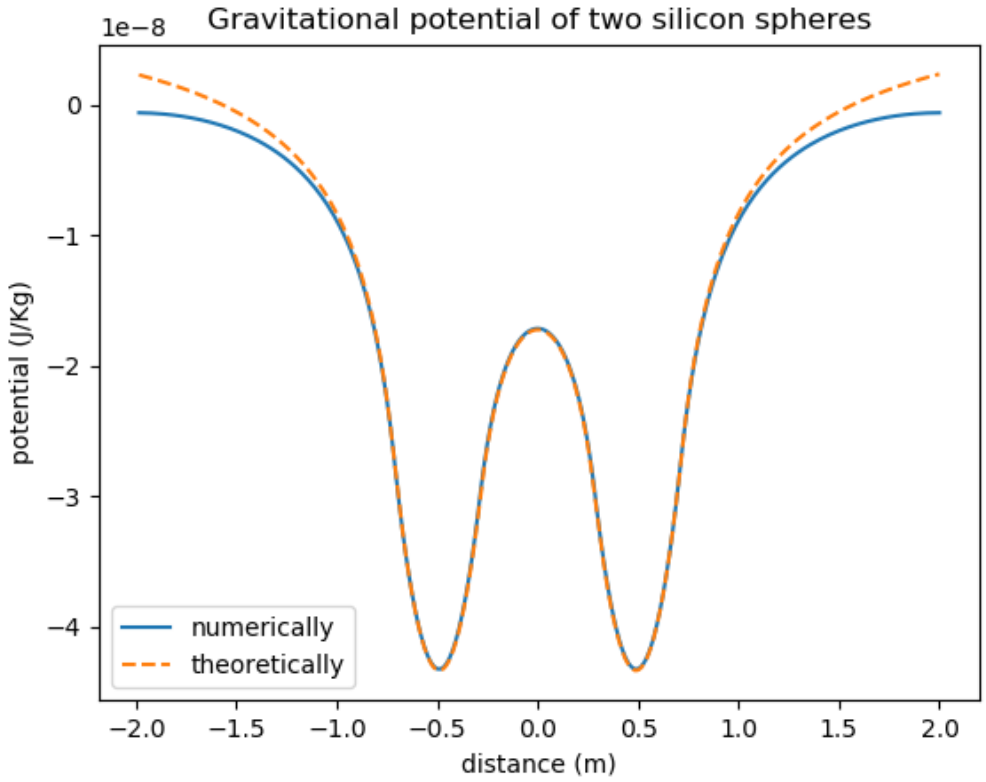

Figure 4: Plot of the potential created by two silicon spheres of 100 kg along a path in the z-direction calculated in two different ways. The blue line represents the potential numerically calculated using the Poisson equation and the DFT. The dashed orange line shows the analytical value of the potential along this line. The two sphere are located at -0.5 m and 0.5 m.

With our obtained expression for ϕ we can now also find the gravitational field $\boldsymbol{g} = -\boldsymbol{\nabla}\phi$, where we use an numerical approximation of the gradient. A second way to calculate the gravitational field is in the Fourier domain. Here we use again that the Fourier transform of the gradient equals $i\boldsymbol{k}$, so $\tilde{\boldsymbol{g}} = i\boldsymbol{k} \cdot \tilde{\phi}$. After this we can get to $\boldsymbol{g}$ using the 3 dimensional inverse FFT on $\tilde{\boldsymbol{g}}$.

Returning to our example, in figure 4 you can see the potential along a line in the z-direction through the potential field caused by our silicon spheres. One is calculated with our discrete method and this is plotted against theoretical values. The line over which we travel is located at x = 0 and y = 0, so going exactly through the center of the spheres. We see that our numerical values are very accurate between the -1 and 1 meters, so in the middle half of the region we simulate. Outside of this region the two potentials start diverging. This effect we have mentioned before and is caused by the DFT which assumes that the values are periodically continued and smooth.

Now that we have the potential and the gravitational field using the Poisson equation from our starting masses, we use this as our starting point to find the potential and the gravitational

field corresponding with these masses from MOND.

4.6. Helmholtz decomposition

In the MOND case we are also able to calculate the potential generated by a mass density distribution with the use of Fourier transforms. However, where the Fourier transform of the Poisson equation is linear, this is not the case for the MOND Poisson equation. As a result, calculating the potential requires some additional steps in this case, in the form of a Helmholtz decomposition. Here we will show what a Helmholtz decomposition consists of and how we can use it to calculate our gravitational potential in the MOND case.

According to Helmholtz's theorem, every sufficiently smooth, rapidly decaying (faster than 1/r), three-dimensional vector field can be written as the sum of a curl-free and a divergence-free vector field. This representation of the original vector field is called its Helmholtz decomposition. In formula form this is written as equation (88), where $\boldsymbol{F}$ is an arbitrary vector field, $\nabla \times \boldsymbol{F}_{\parallel} = 0$ and $\nabla \cdot \boldsymbol{F}_{\perp} = 0$. So here $\boldsymbol{F}_{\parallel}$ is the curl-free part, also called the conservative or irrotational part and $\boldsymbol{F}_{\perp}$ the divergence-free or solenoidal part.

$$\boldsymbol{F} = \boldsymbol{F}_{\parallel} + \boldsymbol{F}_{\perp} \tag{88}$$

As the Fourier transform is a linear map, we have that:

$$\tilde{\boldsymbol{F}} = \tilde{\boldsymbol{F}}_{\parallel} + \tilde{\boldsymbol{F}}_{\perp} \tag{89}$$

However, as we are now working in the Fourier domain we have that $i\boldsymbol{k} \times \tilde{\boldsymbol{F}}_{\parallel} = 0$ and $i\boldsymbol{k} \cdot \tilde{\boldsymbol{F}}_{\perp} = 0$, as $\mathcal{F}\{\nabla\} = i\boldsymbol{k}$. These identities we can use to find the irrotational and the solenoidal parts of any vector field in the Fourier domain. We do this using:

$$\boldsymbol{k}\frac{\boldsymbol{k} \cdot \tilde{\boldsymbol{F}}}{\boldsymbol{k} \cdot \boldsymbol{k}} = \boldsymbol{k}\frac{\boldsymbol{k} \cdot \tilde{\boldsymbol{F}}_{\parallel} + \boldsymbol{k} \cdot \tilde{\boldsymbol{F}}_{\perp}}{\boldsymbol{k} \cdot \boldsymbol{k}} = \boldsymbol{k}\frac{\boldsymbol{k} \cdot \tilde{\boldsymbol{F}}_{\parallel}}{\boldsymbol{k} \cdot \boldsymbol{k}} = \tilde{\boldsymbol{F}}_{\parallel} \tag{90}$$

This we can then use to find $\tilde{\boldsymbol{F}}_{\perp}$ by combining equations (89) and (90).

$$\tilde{\boldsymbol{F}}_{\perp} = \tilde{\boldsymbol{F}} - \tilde{\boldsymbol{F}}_{\parallel} = \tilde{\boldsymbol{F}} - \boldsymbol{k}\frac{\boldsymbol{k} \cdot \tilde{\boldsymbol{F}}}{\boldsymbol{k} \cdot \boldsymbol{k}} \tag{91}$$

These equations we will use to find our potential in the MOND case.

4.7. Calculating potentials in case of deep MOND

Recall the deep MOND-Poisson equation (29), here restated as equation (92).

$$\nabla \cdot \left(\frac{|\nabla \phi_{DM}|}{a_0} \nabla \phi_{DM} \right) = 4\pi G \rho \tag{92}$$

We cannot numerically solve this equation in the same way as in the Newtonian case, as it is nonlinear. Therefore to calculate the gravitational potential from a mass density according to the MOND-Poisson equation we will use an iterative process. Before showing the principles of this process we will first rewrite this equation into a system of more convenient equations.

To do this we will use the similarities that exist between the MOND-Poisson equation (92) and the Newtonian Poisson equation (20), which we have restated in equation (93).

$$\nabla \cdot \nabla \phi_N = 4\pi G\rho \tag{93}$$

We start by defining $\boldsymbol{f}$ as the gravitational acceleration caused by the deep MOND potential and $\boldsymbol{g}$ as the acceleration as a result of the Newtonian potential.

$$\boldsymbol{f} = -\nabla \phi_{DM} \tag{94}$$

$$\boldsymbol{g} = -\nabla \phi_N \tag{95}$$

As both $\boldsymbol{f}$ and $\boldsymbol{g}$ have a potential, we know that they are conservative and therefore that $\nabla \times \boldsymbol{f} = \nabla \times \boldsymbol{g} = \boldsymbol{0}$. Furthermore we define:

$$\boldsymbol{F} = \frac{f}{a_0}\boldsymbol{f} = -\frac{|\nabla \phi_{DM}|}{a_0}\nabla \phi_{DM} \tag{96}$$

$\boldsymbol{F}$ is the vector field on which we will use the Helmholtz decomposition. We will call the curl-free part $\boldsymbol{E}$ and the divergence free-part $\boldsymbol{B}$. So we get:

$$\boldsymbol{F} = \boldsymbol{E} + \boldsymbol{B} \tag{97}$$

$$\nabla \times \boldsymbol{E} = \boldsymbol{0} \tag{98}$$

$$\nabla \cdot \boldsymbol{B} = 0 \tag{99}$$

Substituting equation (95) into the Poisson equation and equations (94) and (96) into the deep MOND-Poisson equation gives us the following formulas:

$$-\nabla \cdot \boldsymbol{g} = 4\pi G\rho \tag{100}$$

$$-\nabla \cdot \boldsymbol{F} = 4\pi G\rho \tag{101}$$

As we know that $\nabla \cdot \boldsymbol{F} = \nabla \cdot \boldsymbol{E} + \nabla \cdot \boldsymbol{B} = \nabla \cdot \boldsymbol{E}$ and that $\boldsymbol{g}$ is conservative, we find that $\boldsymbol{E} = \boldsymbol{g} = -\nabla \phi_N$. If we take all the new equations we can now make a system of four equations of which the solution is equal to the MOND-Poisson equation (92). Note that taking the gradient of equation (102) and substituting all the variables results in the original equation. The last equation is necessary to make sure that our solution for $\boldsymbol{f}$ is still conservative and therefore has a potential field.

$$\boldsymbol{F} = \boldsymbol{g} + \boldsymbol{B} \tag{102}$$

$$\nabla \cdot \boldsymbol{B} = 0 \tag{103}$$

$$\boldsymbol{F} = \frac{f}{a_0}\boldsymbol{f} \tag{104}$$

$$\nabla \times \boldsymbol{f} = \boldsymbol{0} \tag{105}$$

We can now solve this system of equations to find a solution for $\boldsymbol{f}$ and thus for ϕ_{DM}. In the next subchapter we will show how we do this.

4.8. Iterative process for finding solutions in deep MOND

To numerically calculate a solution for $\boldsymbol{f}$ we use an iterative process consisting of two steps. First we will explain how we get the starting values $\boldsymbol{F}_0$ and $\boldsymbol{f}_0$ and then how we iterate with those values to find a sufficiently close solution for $\boldsymbol{f}$.

We define our zeroth order solution by assuming $\boldsymbol{B}_0 = 0$. Then we have that:

$$\boldsymbol{F}_0 = \boldsymbol{g} \tag{106}$$

$$\boldsymbol{f}_0 = \boldsymbol{F}_0\sqrt{\frac{a_0}{F_0}} = \boldsymbol{g}\sqrt{\frac{a_0}{g}} \tag{107}$$

While $\boldsymbol{g}$ is conservative by definition, this is not in general true for $\boldsymbol{f}_0$, so this solution does not generally satisfy our system of equations. An interesting caveat is that for the specific case of a single spherical mass distribution $\nabla \times \boldsymbol{f}_0 = 0$ and therefore no iteration steps are necessary.

Now we have a starting point for our iterative process. As the only problem with our current solution is that $\boldsymbol{f}_0$ is not conservative we use the Helmholtz decomposition to split it in a conservative and a divergence-free part and define $\boldsymbol{f}_1$ as the conservative part.

$$\boldsymbol{f}_0 = \boldsymbol{f}_{0,\parallel} + \boldsymbol{f}_{0,\perp} \tag{108}$$

$$\boldsymbol{f}_1 = \boldsymbol{f}_{0,\parallel} \tag{109}$$

Remember that using equation (90) we can easily calculate the conservative part of a Helmholtz decomposition in the Fourier domain, so we have:

$$\boldsymbol{f}_1 = \boldsymbol{f}_{0,\parallel} = \mathcal{F}^{-1}\{\boldsymbol{k}\frac{\boldsymbol{k}\cdot\tilde{\boldsymbol{f}}_0}{\boldsymbol{k}\cdot\boldsymbol{k}}\} \tag{110}$$

From this we can calculate the value for $\boldsymbol{B}_1$ as in equation (111).

$$\boldsymbol{B}_1 = \boldsymbol{F}_1 - \boldsymbol{g} = \frac{f_1}{a_0}\boldsymbol{f}_1 - \boldsymbol{g} \tag{111}$$

However, this new value for $\boldsymbol{B}_1$ is not curl-free anymore. Thus in the iteration next step we make $\boldsymbol{B}_2$ curl-free again, using the Helmholtz decomposition of $\boldsymbol{B}_1$ and equation (91). We get:

$$\boldsymbol{B}_2 = \boldsymbol{B}_{1,\parallel} = \mathcal{F}^{-1}\{\tilde{\boldsymbol{B}}_1 - \boldsymbol{k}\frac{\boldsymbol{k}\cdot\tilde{\boldsymbol{B}}_1}{\boldsymbol{k}\cdot\boldsymbol{k}}\} \tag{112}$$

No we can calculate $\boldsymbol{f}_2$ from $\boldsymbol{B}_2$ and this is again not conservative anymore. So the entire process starts again and we can give a general definition for our iteration steps. We split this into the definitions for the two different steps. For even n we have:

$$\boldsymbol{f}_{n+1} = \mathcal{F}^{-1}\{\boldsymbol{k}\frac{\boldsymbol{k}\cdot\tilde{\boldsymbol{f}}_n}{\boldsymbol{k}\cdot\boldsymbol{k}}\} \tag{113}$$

$$\boldsymbol{B}_{n+1} = \frac{f_{n+1}}{a_0}\boldsymbol{f_{n+1}} - \boldsymbol{g} \tag{114}$$

And for odd n we have:

$$\boldsymbol{B}_{n+1} = \mathcal{F}^{-1}\{\tilde{\boldsymbol{B}}_n - \boldsymbol{k}\frac{\boldsymbol{k}\cdot\tilde{\boldsymbol{B}}_n}{\boldsymbol{k}\cdot\boldsymbol{k}}\} \tag{115}$$

$$\boldsymbol{f}_{n+1} = (\boldsymbol{g} + \boldsymbol{B}) \sqrt{\frac{a_0}{|\boldsymbol{g} + \boldsymbol{B}|}} \tag{116}$$

Using these iteration steps we can now calculate a value for $\boldsymbol{f}$, from which we can then also calculate the deep MOND potential ϕ_{DM}. The only thing we still have to define is a condition for when our iteration process had converged close enough to the truth to be reliable. As we are not converging to theoretic values we define our iterative process as complete when the calculated value for f is within 0.1% of the previous value, so $\left|\frac{f_{n+1}}{f_n}\right| < 0.001$.

4.9. Apparent and dark matter

In our model we initially only use the baryonic mass of galaxies in our mass density distribution, as according to the MOND theory there is no dark matter. However, we can use our model to show where you would be able to see 'dark matter' if you looked at our gravitational potential while assuming that standard Newtonian dynamics hold. This is done to see where dark matter could be detected in this case, so we can see if it corresponds with current literature, as that would mean that it could be explained by MOND. Here we will explain how we calculate this dark matter distribution.

We start with a deep MOND gravitational potential ϕ_{DM} calculated with the iterative process described above. Then using the Poisson equation (20) we can find an apparent mass density ρ_{App}. To avoid confusion we will call the baryonic mass density ρ_{Bar} from now on. In equation (117) we have restated the Poisson equation with the variables used here.

$$\nabla \cdot \nabla \phi_{\text{DM}} = 4\pi G \rho_{\text{App}} \tag{117}$$

The resulting mass density ρ_{App} is thus the mass density that would with Newtonian dynamics cause the potential we find from ρ_{Bar} with deep MOND. We define the difference between these two mass densities as the dark matter distribution $\rho_{\text{Dark}} = \rho_{\text{App}} - \rho_{\text{Bar}}$. ρ_{Dark} contains all the matter that according to Newtonian dynamics we would expect to exist, but we cannot see. In the next chapter we will extensively look into these three densities.

4.10. Projected clusters

As previously mentioned in the introduction, astronomers use gravitational lensing events as a way to observe the potential field of galaxy clusters and find matter distributions in clusters. This is something that could be compared to the apparent mass distributions we find using MOND. However, galaxies cannot be given a 3 dimensional position inside an observed cluster, as the precise distance to earth often cannot be determined. Instead astronomers observe the 2 dimensional projection of galaxy clusters. This means that they look at the projection of the galaxy cluster on a 2d plane. As a result, estimated mass distributions of galaxy clusters are also calculated as 2d distributions, in kg/m^2. To simulate this we will also calculate the 2d projections of the apparent, dark and baryonic mass densities resulting from our simulations. We will do this by summing our mass density matrix over the z-axis and multiplying with the length of one discrete volume to get the area densities ρ_A.

5. Results and discussion

5.1. Example galaxy

We start by showing some images made in Python of an example galaxy to better show what the simulated clusters and their potentials look like. We do this by showing slices of an example cluster for 4 different functions. These variables are the initial baryonic mass density distribution, the Newtonian gravitational potential, the deep MOND gravitational potential and the apparent mass density distribution. For all figures 15 slices are taken in the z-plane between $z = -0.7$ Mpc and $z = 0.7$ Mpc with a distance of 0.1 Mpc between slices. Note that we do not show the entire region we have modelled, which goes from -1 Mpc to 1 Mpc in all directions, as distortions resulting from the DFT are visible around the edges.

The first variable, the initial mass density distribution, is shown in figure 5. As we have modelled the mass density inside of the galaxies as constant, we see that there are only two distinct values in the figure, the density of a galaxy, $\rho = 7.12 \cdot 10^{-23}$ Kg/m^3 inside all galaxies and a density of zero outside. All galaxies have the same radius $r = 30$ Kpc, but, as their center is randomly chosen, it isn't always in the middle of a region we use for our discretization. This explains why some galaxies seem to have a slightly different shape. The shown galaxy cluster consists of 100 galaxies, but not all galaxies are visible in this figure. This is a result of the fact that the galaxies are small enough to lay in between two slices. Furthermore, as the distribution function we use has no upper distance limit, a small percentage of galaxies can be located outside the plotted and sometimes even outside the modelled region.

Secondly, the gravitational potential calculated with standard Newtonian dynamics is shown in figure 6. We see that the potential is lowest inside the galaxies and especially low in galaxies close together in the center of the cluster. Around this there is a cloud of moderate potential-values around the center, which becomes higher further away from the center.

The third funciton we look at is the gravitational potential calculated using deep MOND, shown in figure 7. Some differences compared with the potential calculated with Newtonian dynamics are clearly visible. For example, the exact locations of the galaxies are a lot more difficult to spot. This is a result of the fact that according to deep MOND the potential decreases by $1/r$ when travelling away from a mass, compared to $1/r^2$ in Newtonian dynamics. This results in the cloud around the center of the cluster having a relatively much lower potential then in the Newtonian case.

Lastly we have plotted the apparent mass distributions in figure 8. Although the centers of the galaxies are still on the same location, galaxies are bigger in the apparent matter distribution. On some locations were in figure 5 no mass was located, now faint circles of low density are visible. This is a result of the fact that the region around a galaxy were apparent mass is located larger is than were baryonic mass is located. This makes galaxies that previously lay between two slices visible. Also, the peak mass density in the center of galaxies is much higher than for the baryonic mass density. We will look more into these effects further in the results. If we look closely we notice that oscillating crosses of mass density can be seen originating from galaxies. This is probably an artifact of the discrete Fourier transforms we use. However, as the densities in these crosses are relatively small, this does not cause problems when further analysing the data.

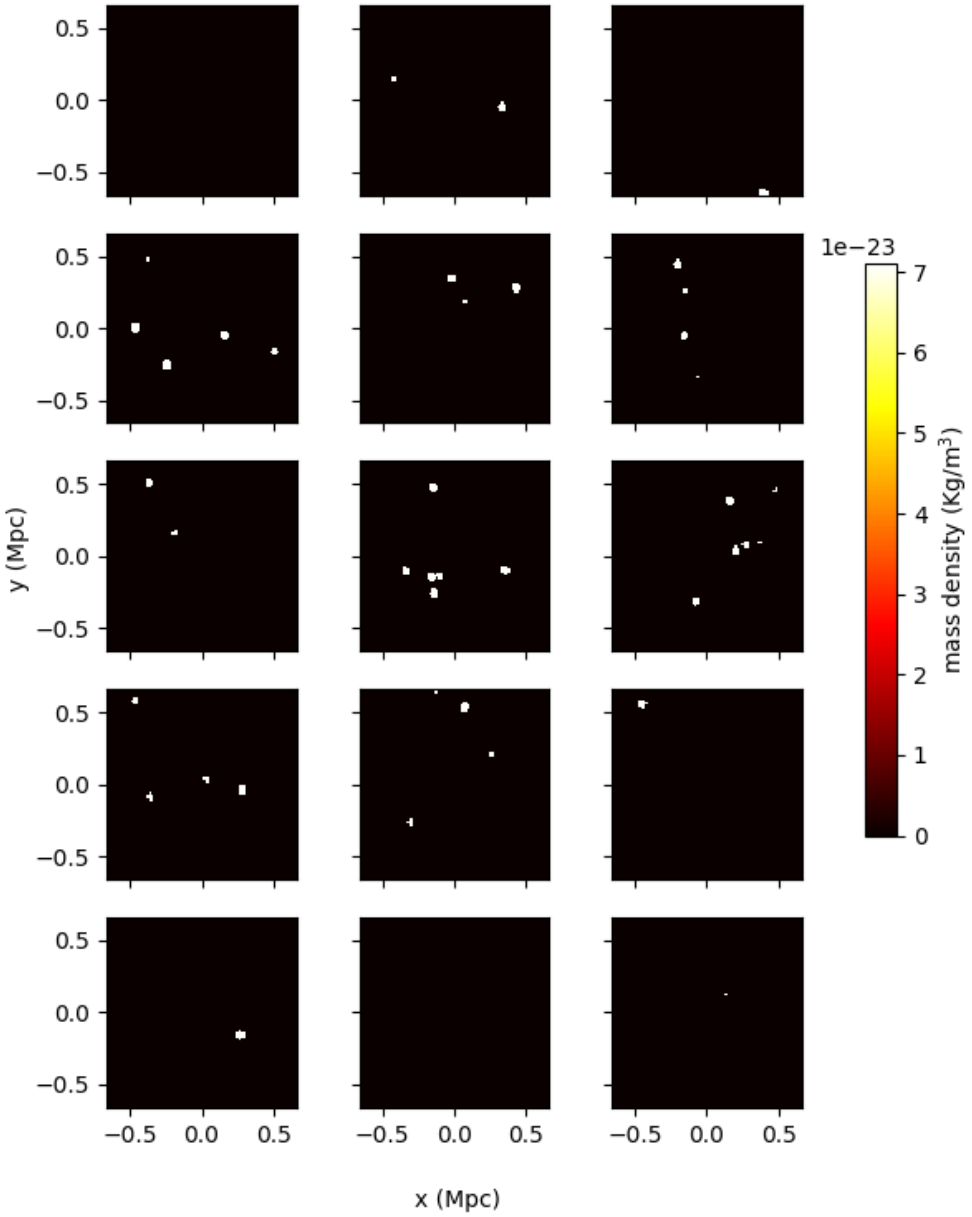

Figure 5: A false colour map of mass density against x and y location in 15 slices of an example cluster. The galaxies in the cluster are distributed according to the isothermal spherically symmetric MOND distribution. The cluster that is shown contains 100 galaxies.

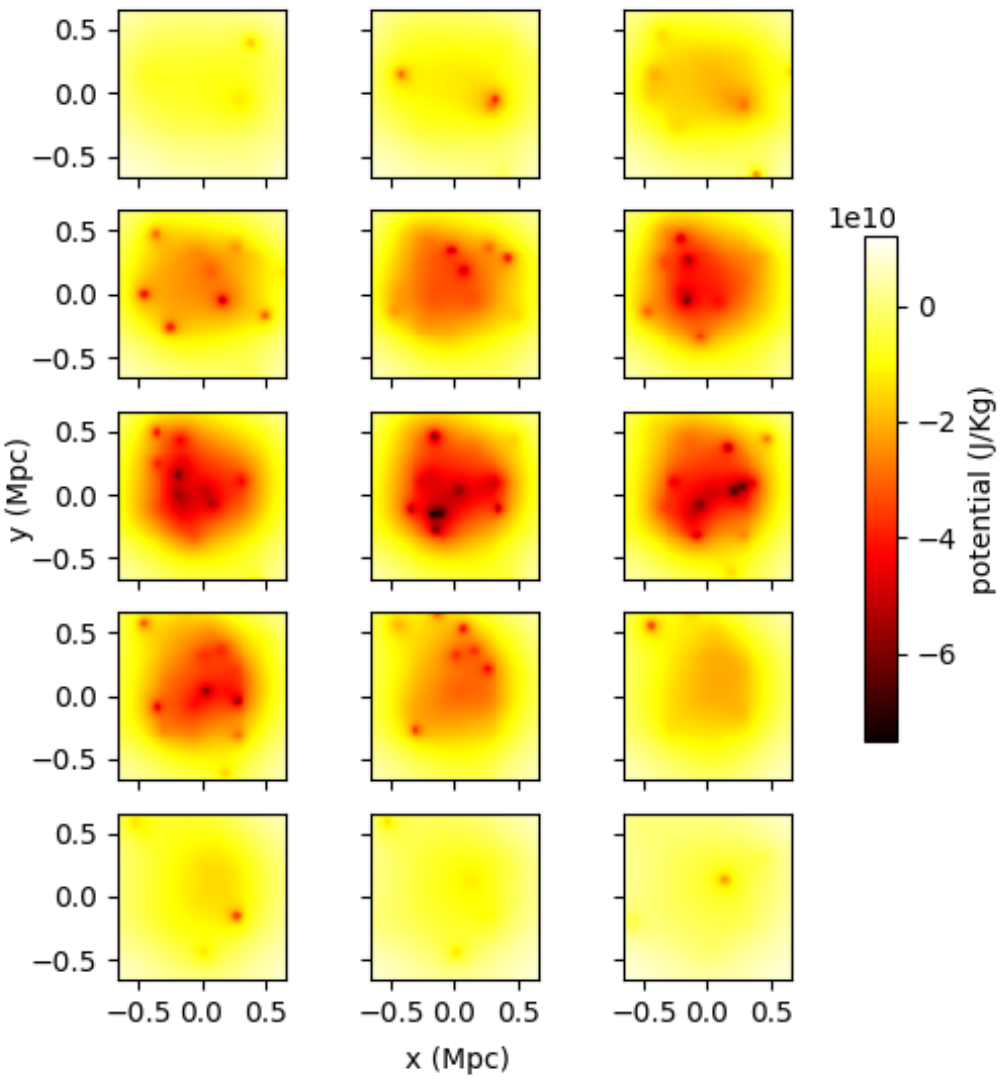

Figure 6: A false colour map of potential against x and y location in 15 slices of an example cluster. The potential shown in this image is calculated form the previous shown mass distribution using standard Newtonian dynamics. The galaxies in the cluster are distributed according to the isothermal spherically symmetric MOND distribution. The cluster that is shown contains 100 galaxies.

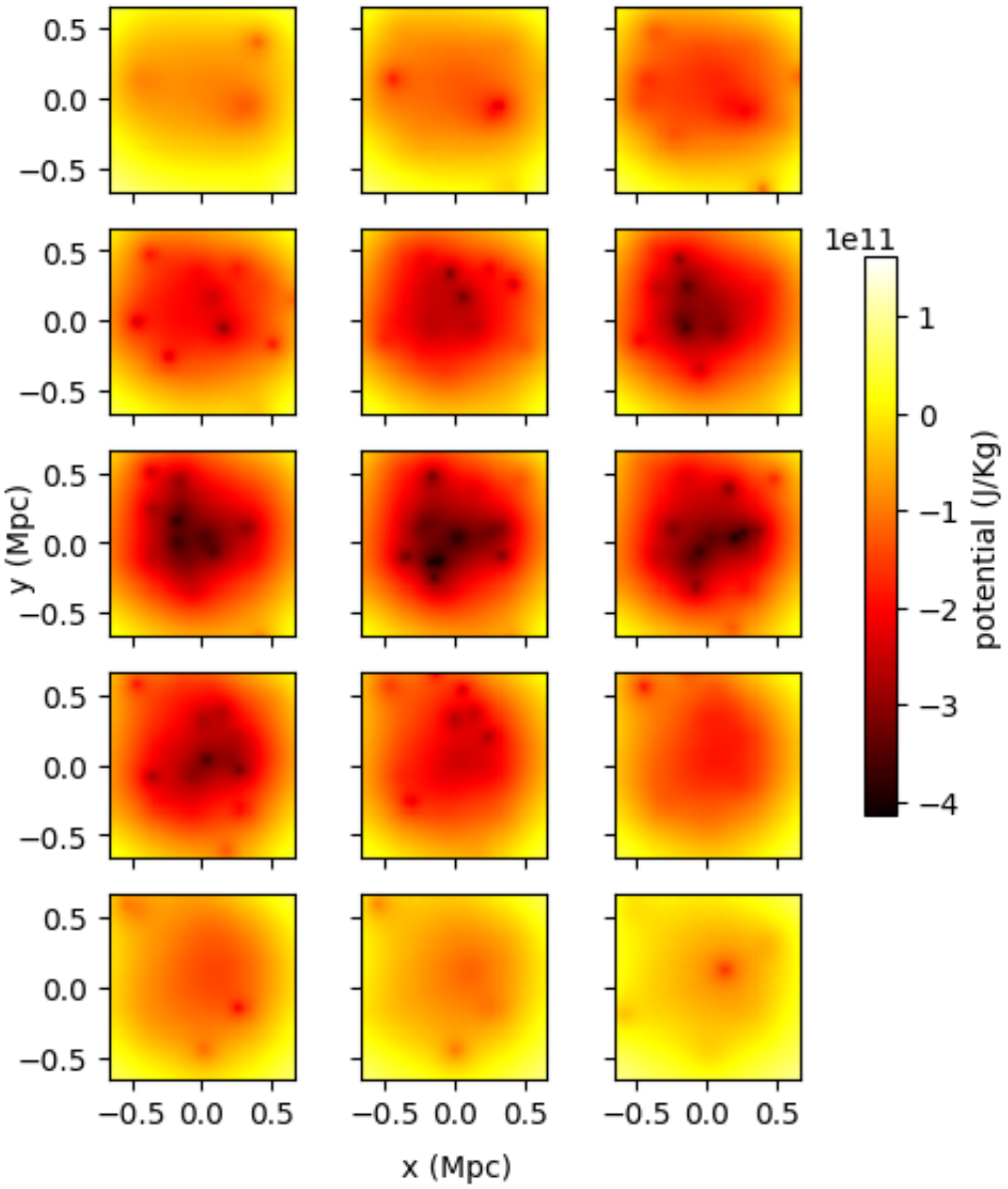

Figure 7: A false colour map of potential against x and y location in 15 slices of an example cluster. The potential shown in this image is calculated form the previous shown mass distribution using MOND. The galaxies in the cluster are distributed according to the isothermal spherically symmetric MOND distribution. The cluster that is shown contains 100 galaxies.

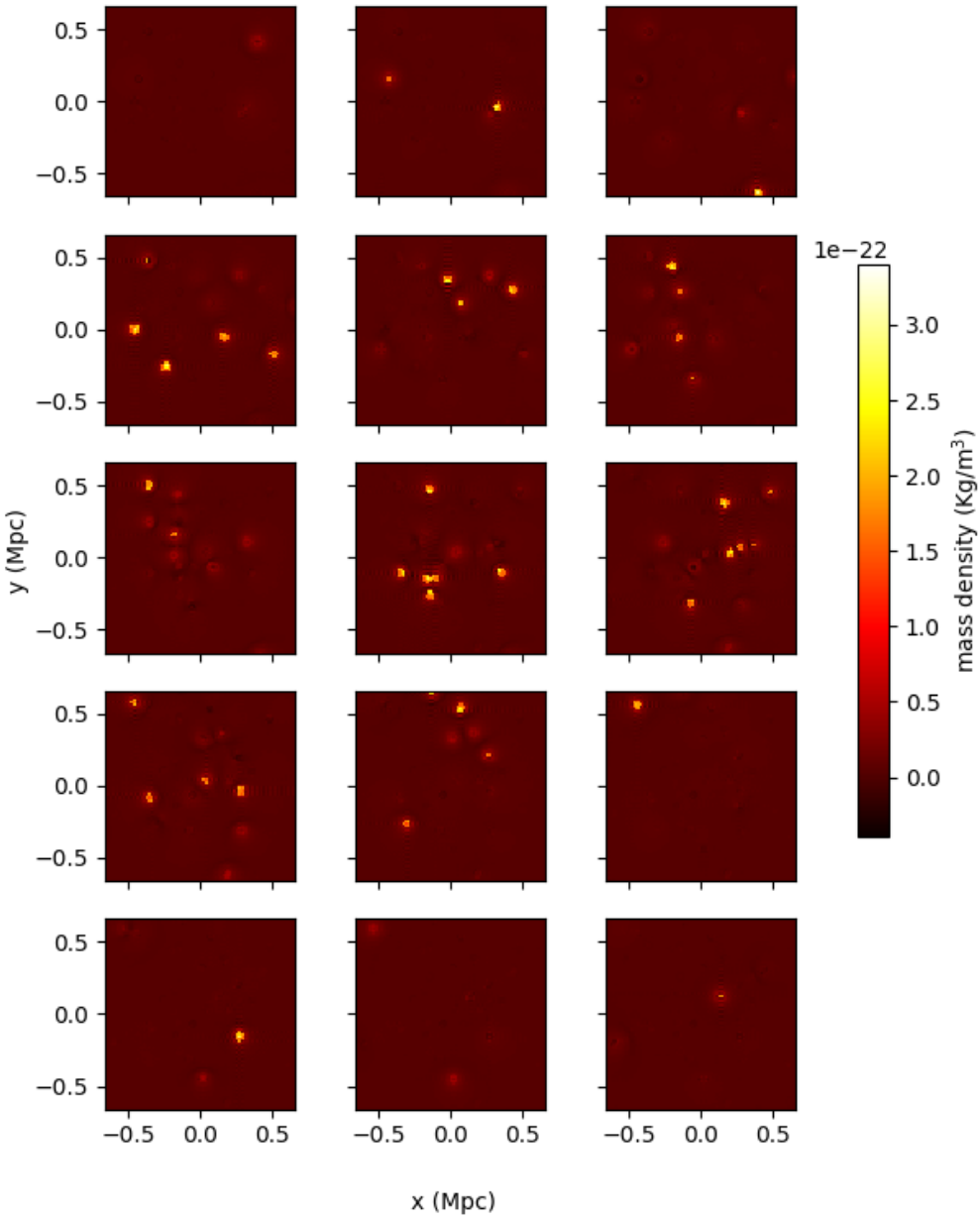

Figure 8: A false colour map of the apparent mass density against x and y location in 15 slices of an example cluster. The galaxies in the cluster are distributed according to the isothermal spherically symmetric MOND distribution. The cluster that is shown contains 100 galaxies.

5.2. Verification of our usage of deep MOND

An important condition for the deep MOND regime is that the absolute value of the acceleration $\boldsymbol{g} = -\nabla\phi_N$ is much smaller than Milgroms constant $a_0 = 1.2 \cdot 10^{-10}$ m/s^2. To check this condition we calculate the maximum value for $g = |\boldsymbol{g}|$ for a simulation with 50 and a simulation with 1000 galaxies, as those are the smallest and largest clusters we will be looking at. We have that $g_{\text{max},50} = 5.941 \cdot 10^{-11}$ m/s^2 $= 0.4575 \cdot a_0$ and $g_{\text{max},1000} = 1.002 \cdot 10^{-10}$ m/s^2 $= 0.8350 \cdot a_0$. To further illustrate this figures 9 and 10 show the values g in the middle slice of a simulation with respectively 50 and 1000 galaxies. So we have that for both clusters it holds everywhere that $g < a_0$, but not that $g \ll a_0$ everywhere. We can still use deep MOND for both clusters, as $g < a_0$ makes MOND still a reasonable assumption. For the cluster with 50 galaxies we are relatively closer to $g \ll a_0$ than for the cluster with 1000 galaxies, so our usage of deep MOND is more accurate for small clusters.

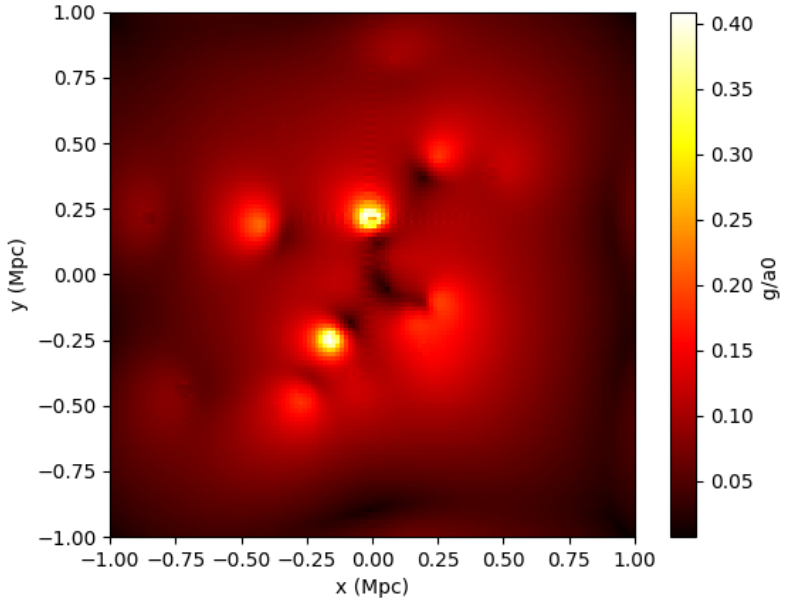

Figure 9: A false colour map of the gravitational acceleration $|\boldsymbol{g}|$ divided by Milgroms constant a_0 against the x and y location in the middle slice, $z = 0$, of an example cluster. The cluster that is shown contains 50 galaxies.

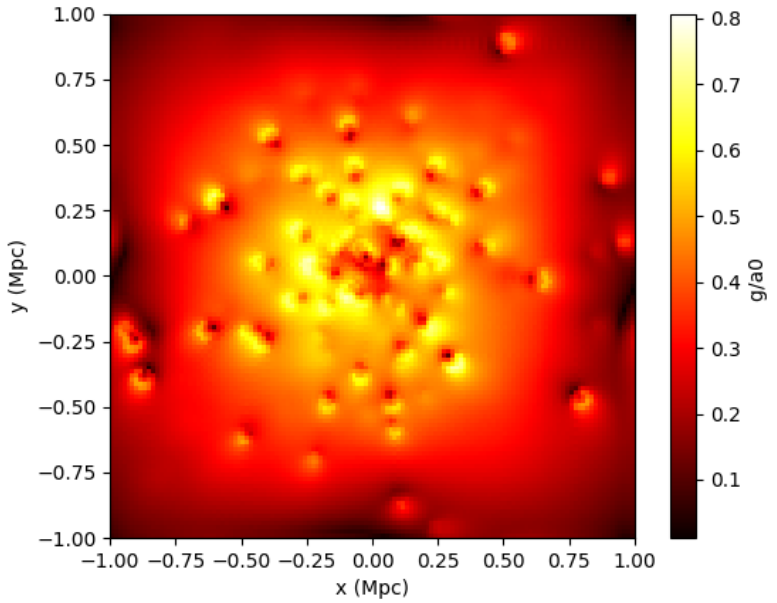

Figure 10: A false colour map of the gravitational acceleration $|\boldsymbol{g}|$ divided by Milgroms constant a_0 against the x and y location in the middle slice, $z = 0$, of an example cluster. The cluster that is shown contains 1000 galaxies.

5.3. Mass ratio

One thing we looked at was the effect of the number of galaxies in a cluster, especially how it would impact the amount of apparent matter. To get a good image of this we ran several simulations for clusters with 10 different numbers of galaxies, $N = 50$, 75, 100, 150, 200, 300, 400, 500, 750 and 1000. For almost all of different clusters we ran 25 simulations. For the two biggest clusters, containing 750 and 1000 galaxies, we ran only 15 and 10 simulations respectively, as it would other wise be too computationally intensive.

For all these simulations the mass and size of a single galaxy and the size of the cluster remains constant. This means that by increasing the number of galaxies we are also increasing the total amount of mass in the cluster and the average density. We calculated the total apparent, dark and baryonic mass in the cluster by summing over the mass in the center half of the region, so all points for which $|x| < 0.5$ Mpc $\wedge$ $|y| < 0.5$ Mpc $\wedge$ $|z| < 0.5$ Mpc. We took this cutoff as this is the region on which we know the DFT has reliable results.

For all these clusters we looked at the ratio between the total amount of dark matter and the total amount of baryonic matter, $\frac{M_{\text{Dark}}}{M_{\text{Bar}}}$. In figures 11 and 12 the average ratio is plotted against the number of galaxies in respectively a normal plot and a plot with logarithmic x- and y-axes. For each point error bars showing the standard deviation are included in the plots. We can see that if the number of galaxies in a cluster increases, $\frac{M_{\text{Dark}}}{M_{\text{Bar}}}$ decreases. This relation looks a lot like a $1/\sqrt{x}$ relation. To check this we tried to fit a curve through these points using a least squares fit. We fitted the data to equation (118).

$$\frac{M_{\text{Dark}}}{M_{\text{Bar}}} = a + \frac{b}{\sqrt{N}} \tag{118}$$

Here N is the number of galaxies in the cluster and a and b are the variables for which we fit. We found $a = 0.8064 \pm 0.2383$ and $b = 101.9 \pm 4.3$. We have $M_{\text{Bar}} = NM_{\text{Gal}}$, with M_{Gal} the mass of a single galaxy, so if $M_{\text{Bar}} \propto N$ we know that $M_{\text{Dark}} \propto aN + b\sqrt{N}$.

The cutoff we used for the region over which we summed the mass probably has some influence on these results. As apparent dark matter is on average seen further away from the center of galaxies than baryonic matter the ratio would probably be slightly smaller if a larger cutoff would have been used. However, the general shape of the relation found would not change as a result of this, as this cutoff is the same for clusters with a different number of galaxies.

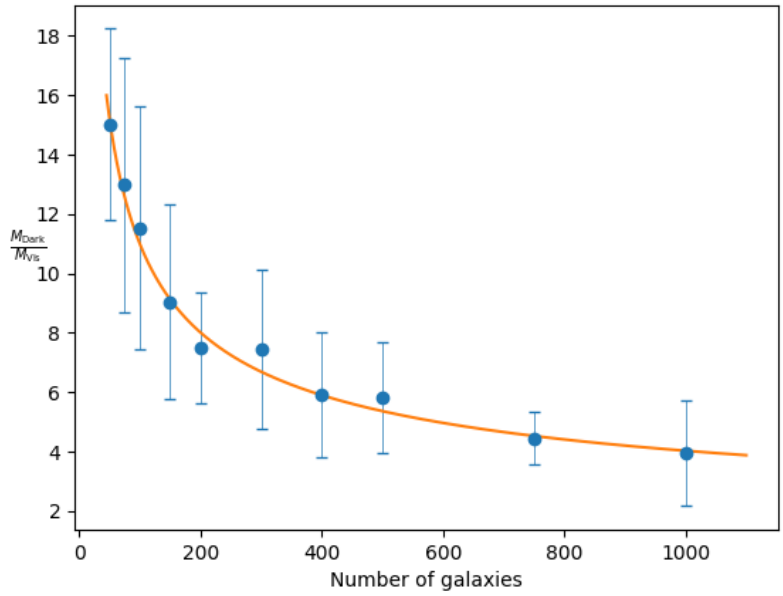

Figure 11: The average ratio between the amount of dark matter and baryonic matter in a galaxy cluster against the number of galaxies N in that cluster. Also included is a curve obtained from a least squares fit through these points.

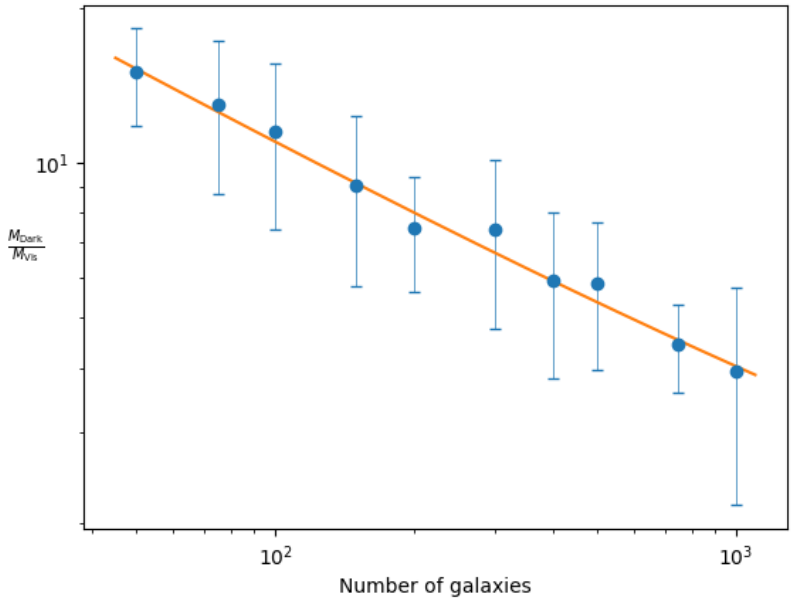

Figure 12: The average ratio between the amount of dark matter and baryonic matter in a galaxy cluster against the number of galaxies N in that cluster plotted with logarithmic x- and y-axes. Also included is a curve obtained from a least squares fit through these points.

5.4. Matter distribution

5.4.1. Mass in concentric spheres around galaxies

Another thing we have looked at in our simulation results is the distribution of baryonic matter, dark matter and total apparent matter around galaxies. This can give us a good idea of where in the neighbourhood of a galaxy supposed dark matter could possibly be explained by MOND. To look at this we take spheres around the center of a galaxy and calculate the total amount of mass inside that sphere. More specifically, we take 100 different radii, $r_0, r_1, ..., r_{100}$, where $r_n = n \cdot 0.0033$ Mpc. Then for every radius we calculate the total amount of baryonic mass M_{Bar} and apparent mass M_{App} inside the sphere with that radius. We do this by summing the densities of all the points inside the sphere multiplied with the the volume of each region in the discrete grid. From this we can also easily calculate the apparent dark matter, $M_{\text{Dark}} = M_{\text{App}} - M_{\text{Bar}}$.

We can now do this for every galaxy in a simulation and then take the average to get the average mass inside a sphere of a certain radius. The reason why we look at the average instead of the individual values is that we average out unexpected results due to odd galaxy placements, like partially overlapping galaxies. Now we can plot the mass inside the radius against the radius to look at what happens. In figure 13 this plot is shown for 25 clusters with 50 galaxies. For each cluster the average apparent, dark and baryonic matter in a radius around a galaxy is plotted against the radius. Furthermore the average over all simulations is also included.

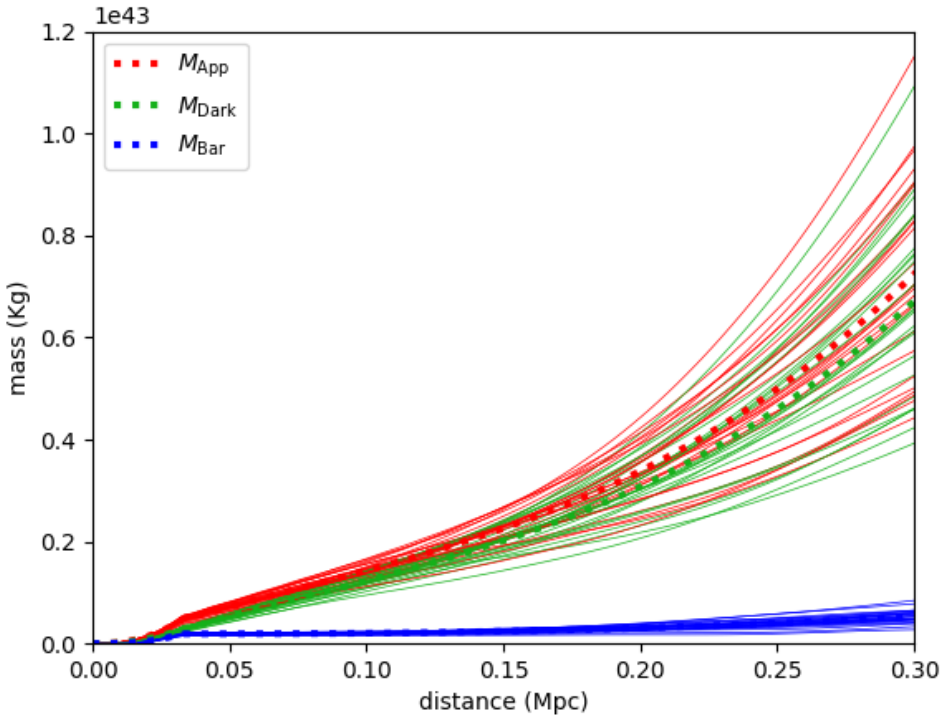

Figure 13: The average apparent, dark and baryonic matter inside a sphere around the center of a galaxy is plotted against the radius of the sphere. This is done for 25 simulations of clusters with 50 galaxies each. Furthermore the average between the simulations is also included as the bold dashed curve.

Note that the average visibly matter increases until about 0.03 Mpc, where we are still inside the galaxy, and then remains constant until about 0.15 Mpc, as no baryonic matter is present outside of the galaxies. Further away, the amount of baryonic matter starts increasing again, as a result of other galaxies in the cluster that are now inside the radius. There the results are way more impacted by the exact placements of the galaxies in the cluster and therefore the average is less useful. This effect is also very visible in the curves showing the apparent matter and the dark matter. We see that the results of the different simulations remain following the same pattern until about 0.15 Mpc, after which they start diverging heavily. Note that this spread in total apparent matter is something we already observed when looking at the ratios of apparent and baryonic mass, which also had a large spread between values.

In figure 14 the same curves are plotted as in figure 13, but the figure is now zoomed in to only show the radii up to 0.1 Mpc. As a result we can more clearly see what happens around a galaxy before the influence of other galaxies start to significantly matter. One interesting observation is that after we have exited the galaxy M_{App}, and as result also M_{Dark}, increases linearly. Furthermore we see that even inside the galaxy a significant amount of apparent dark matter is predicted.

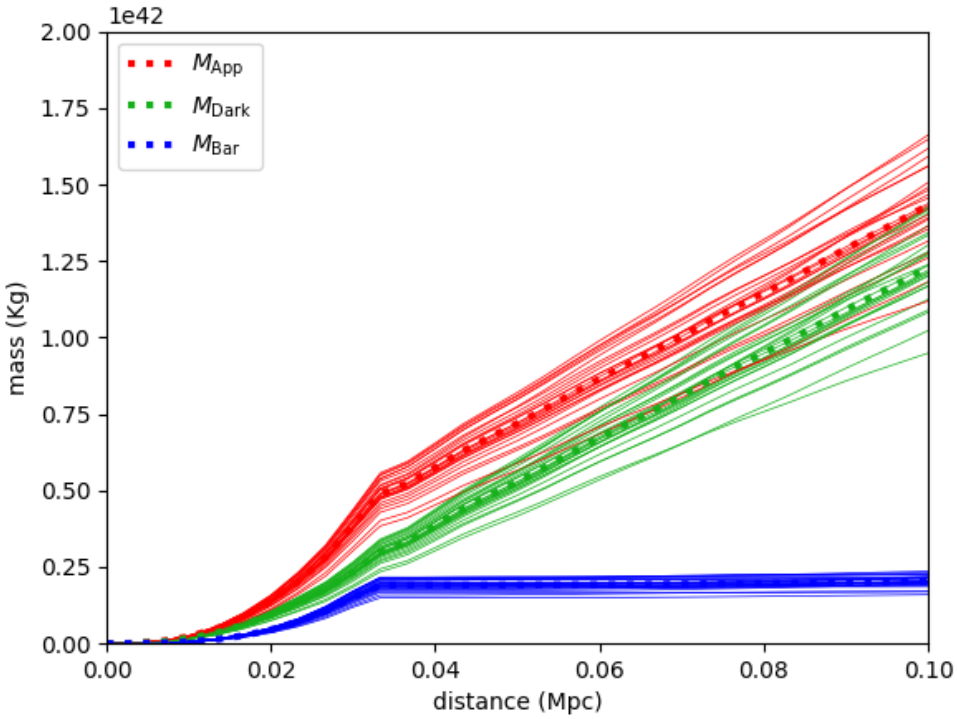

Figure 14: The average apparent, dark and baryonic matter inside a sphere around the center of a galaxy is plotted against the radius of the sphere. This is done for 25 simulations of clusters with 50 galaxies each. Furthermore the average between the simulations is also included as the bold dashed curve. This figure in a zoomed in version of figure 13 .

In figures 15 and 16 the same plots are shown for 25 clusters containing 500 galaxies. As there are now a lot more galaxies in the same volume, they are on average closer to another. We see that this immediately results in a higher amount of apparent and baryonic matter at large radii. Therefore the zoomed in version gives us more information in this case. We see that the amount of baryonic matter starts increasing again already at a radius of 0.05 Mpc, just outside the initial galaxy.

Once more we see that the apparent mass curve has three main phases. We will try to define these phases more clearly. In the first phase we are still inside the initial galaxy and the average apparent matter seems to increase quadratically. Then, upon exiting the galaxy, a clear bend is visible, after which it increases linearly. This lasts until other nearby galaxies start affecting the amount of apparent mass. Lastly, in phase three, the effects of these nearby galaxies causes again a seemingly quadratic increase in apparent matter. The location where the shift from phase two to phase three occurs depends heavily on the number of galaxies in the cluster.

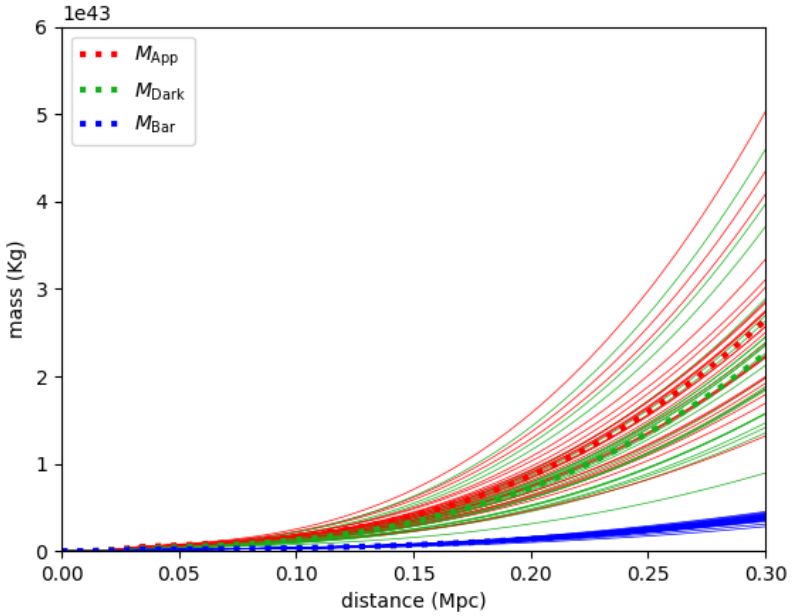

Figure 15: The average apparent, dark and baryonic matter inside a sphere around the center of a galaxy is plotted against the radius of the sphere. This is done for 25 simulations of clusters with 500 galaxies each. Furthermore the average between the simulations is also included as the bold dashed curve.

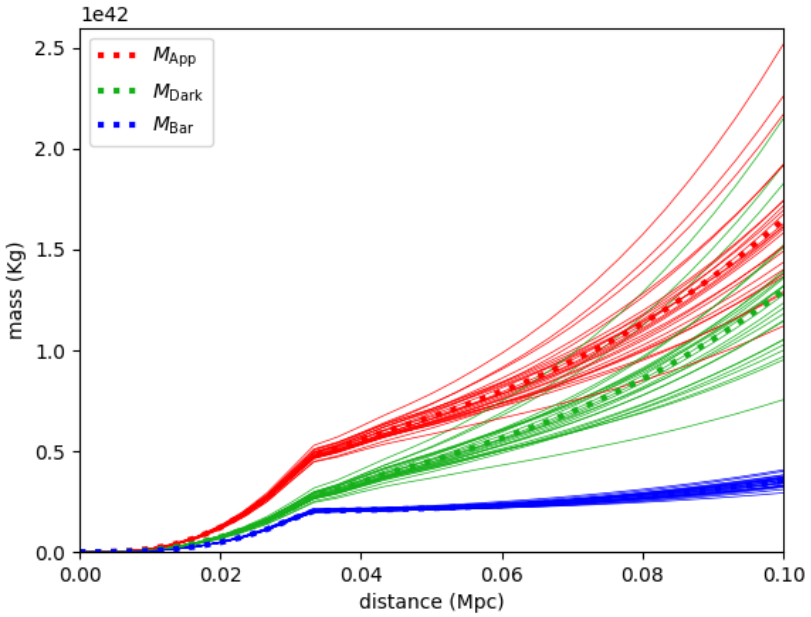

Figure 16: The average apparent, dark and baryonic matter inside a sphere around the center of a galaxy is plotted against the radius of the sphere. This is done for 25 simulations of clusters with 500 galaxies each. Furthermore the average between the simulations is also included as the bold dashed curve. This figure in a zoomed in version of figure 15 .

We will now take a closer look at the seemingly linear increase in apparent mass in phase two and compare it to theoretical values. For the theoretical comparison we assume that in phase two the gravitational acceleration $\boldsymbol{g}_{\text{DM}}$ is only influenced by the initial galaxy. Recall that the gravitational acceleration as a result of a point mass according to deep MOND is give by equation (119), which is equation (27) restated using the current variable names.

$$|\boldsymbol{g}_{\text{DM}}| = \frac{\sqrt{GM_{\text{G,Bar}}a_0}}{r} \tag{119}$$

Here $M_{\text{G,Bar}}$ is the baryonic mass of a single galaxy. As we are outside the initial galaxy and not influenced by other galaxies, $M_{\text{G,Bar}}$ is constant relative to the radius r. The apparent mass M_{App} was defined as the mass that caused the same potential, and thus also the same gravitational acceleration $\boldsymbol{g}_{\text{DM}}$, using the Newtonian Poisson equation. Assuming the apparent mass is distributed spherically symmetric, we can then use that the acceleration at a distance r to a galaxy is only influenced by all mass inside the radius r. We define $M_{\text{App}}(r)$ as the apparent mass in a sphere with radius r around the galaxy. Then for the gravitational acceleration $|\boldsymbol{g}_{\text{DM}}|$ the following must also hold:

$$|\boldsymbol{g}_{\text{DM}}| = \frac{GM_{\text{App}}(r)}{r^2} \tag{120}$$

As both values for $|\boldsymbol{g}_{\text{DM}}|$ must be equal, we have:

$$M_{\text{App}}(r) = \sqrt{\frac{M_{\text{G,Bar}}a_0}{G}}\ r \tag{121}$$

So the slope of the curve for apparent mass in phase two is theoretically defined as (122).

$$\frac{dM_{\text{App}}(r)}{dr} = \sqrt{\frac{M_{\text{G,Bar}}a_0}{G}} = 6.0 \cdot 10^{20}\ \text{Kg/m} \tag{122}$$

Here we used the average value for $M_{\text{G,Bar}}$ from figure 14, $M_{\text{G,Bar}} = 2.0 \cdot 10^{41}$ Kg. We can now compare this to the slope of the average apparent mass we see in figure 14. There we have just outside the initial galaxy that $M_{\text{App}}(0.033\ \text{Mpc}) = 4.9 \cdot 10^{41}$ Kg. Further away, near the transition to phase three, we have that $M_{\text{App}}(0.099\ \text{Mpc}) = 1.4 \cdot 10^{42}$ Kg. This gives a slope of $\frac{dM_{\text{App}}(r)}{dr} = \frac{9.1 \cdot 10^{41}\text{Kg}}{0.066\ \text{Mpc}} = 4.5 \cdot 10^{20}$ Kg/m. We can do the same for the cluster with 500 galaxies in figure 16, the only difference being that we have to take a smaller interval as other galaxies start influencing the data earlier. The theoretical value for the slope stays the same. We now have $M_{\text{App}}(0.033\ \text{Mpc}) = 4.8 \cdot 10^{41}$ Kg and $M_{\text{App}}(0.050\ \text{Mpc}) = 6.7 \cdot 10^{41}$ Kg, giving $\frac{dM_{\text{App}}(r)}{dr} = \frac{1.9 \cdot 10^{41}\text{Kg}}{0.017\ \text{Mpc}} = 3.6 \cdot 10^{20}$ Kg/m. For both plots we find that the slope coming from the model is in the same order of magnitude of the theoretical value. They do not give exactly the same value but that might be a logical consequence of the amount of assumptions we made calculating the theoretical value.

5.4.2. Mass densities around galaxies

Next to the total matter we also looked at how the average apparent, dark and baryonic matter densities, ρ_{App}, ρ_{Dark} and ρ_{Bar} , relate to the distance to the center of a galaxy. We calculate this using the values we also used in our previous calculations about total matter distribution. We now take half as much radii, so we have $r_0, r_1, ..., r_{50}$, where $r_n = n \cdot 0.0066$ Mpc. The reason

we take half the radii is because we are looking at discrete regions and without doing this it can happen that, relatively, a lower amount of discrete regions are in one sphere shell than in the next, distorting the data. A lower sample size makes the data more smooth. Now we define the following formula for calculating the average mass density between two radii for which we know the mass in the corresponding sphere.

$$\rho\left(\frac{r_i + r_{i+1}}{2}\right) = \frac{3\left(M_{i+1} - M_i\right)}{4\pi\left(r_{i+1}^3 - r_i^3\right)} \tag{123}$$

In figures 17 and 18 the average mass density, averaged over all galaxies in one cluster and over all 25 simulations, is plotted against distance for the simulations with 50 and 500 galaxies respectively. We see that for the simulations with 50 galaxies the baryonic mass density ρ_{Bar} is a constant value and then drops to almost zero as we leave the galaxy. Note that at the edge of the initial galaxy there is one sphere shell that lays partly inside and partly outside the galaxy, resulting in the one data point between the constant and the almost zero values. We see that the dark matter density looks much more like a continuous function then the apparent and baryonic mass densities. While the highest concentrations of dark matter are found at the center of the galaxy, it decreases smoothly when we exit the galaxy.

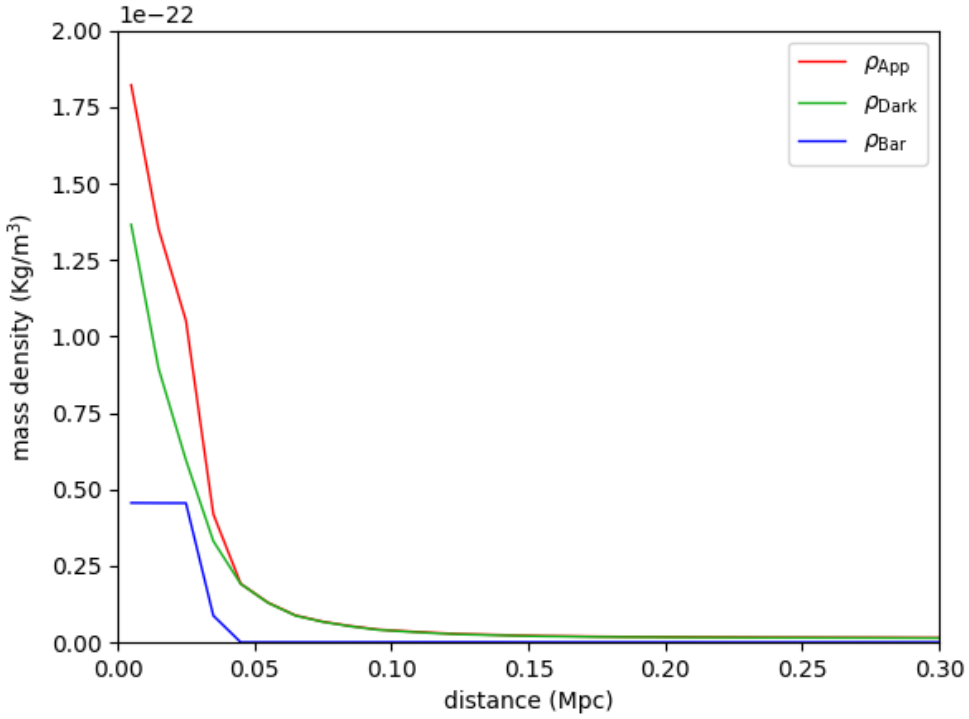

Figure 17: The average apparent, dark and baryonic mass density against the distance from a galaxy inside a cluster of 50 galaxies. All values are an average over 25 simulations of the average over all galaxies inside a single cluster.

In figure 18 the same data is plotted for the average of 25 clusters containing 500 galaxies. We see that the curve for ρ_{Bar} has the same shape as in the previous plot. The only difference is that it stays more noticeably above zero outside the initial galaxy, as a result of more galaxies

and thus a higher chance of them being in closer proximity. An other interesting observation is that the maximum densities of apparent and dark matter and also the shape of the curves are significantly different between the simulations with 50 and 500 galaxies. In the case of 50 galaxies the rate with which ρ_{Dark} increases keeps increasing how closer you get to the center. The opposite seems to be the case for clusters with 500 galaxies, the curve for ρ_{Dark} flattens out a bit when the distance to the center goes to zero.

We also notice that in both plots further away from the center the average apparent and dark mass density seem to go to a constant value. This isn't the case however. You can see in figures 19 and 20, which are zoomed in versions of figures 17 and 18, that ρ_{Dark} and ρ_{App} decrease seemingly linearly after a certain point. The point were it changes from an quadratic to a linear decrease seem to be almost equal to where the baryonic mass started increasing in figures 14 and 16. So from that point the effects of the dark matter of other galaxies also start influencing the dark matter density, changing the rate in which it decreases. This corresponds with the shift between phase two and three we saw in the plots for total apparent matter.

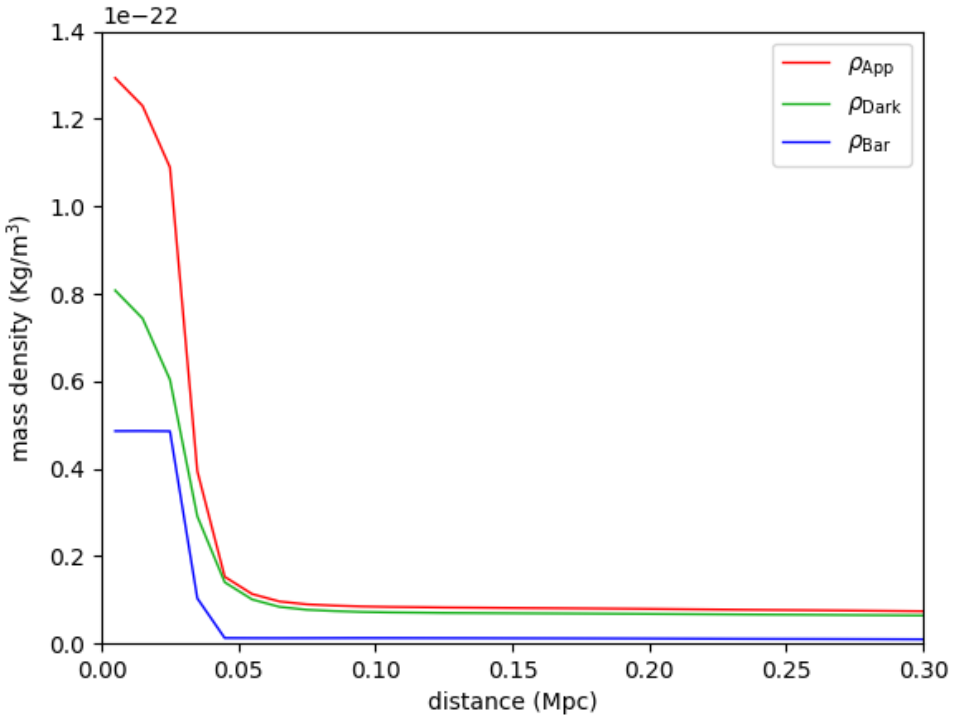

Figure 18: The average apparent, dark and baryonic mass density against the distance from a galaxy inside a cluster of 500 galaxies. All values are an average over 25 simulations of the average over all galaxies inside a single cluster.

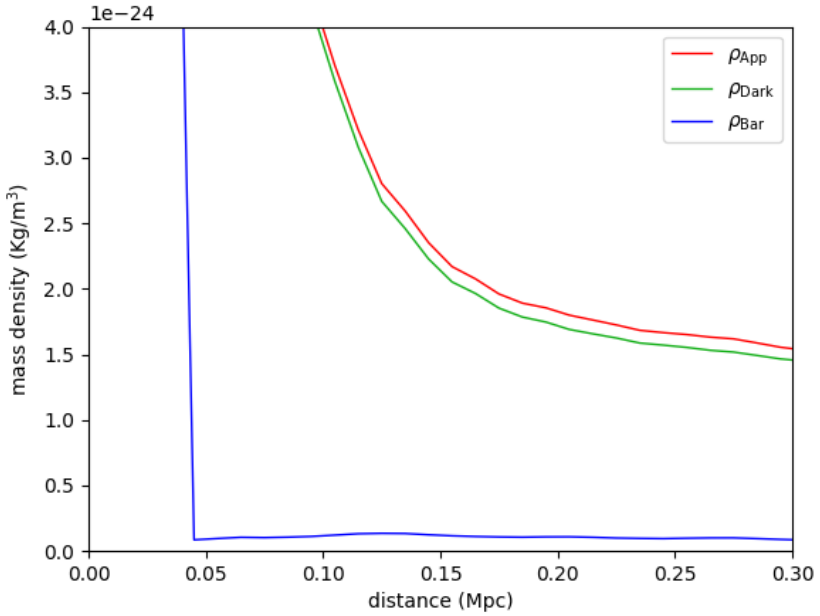

Figure 19: The average apparent, dark and baryonic mass density against the distance from a galaxy inside a cluster of 50 galaxies. All values are an average over 25 simulations of the average over all galaxies inside a single cluster. This figure is an in the y-direction zoomed in version of 17.

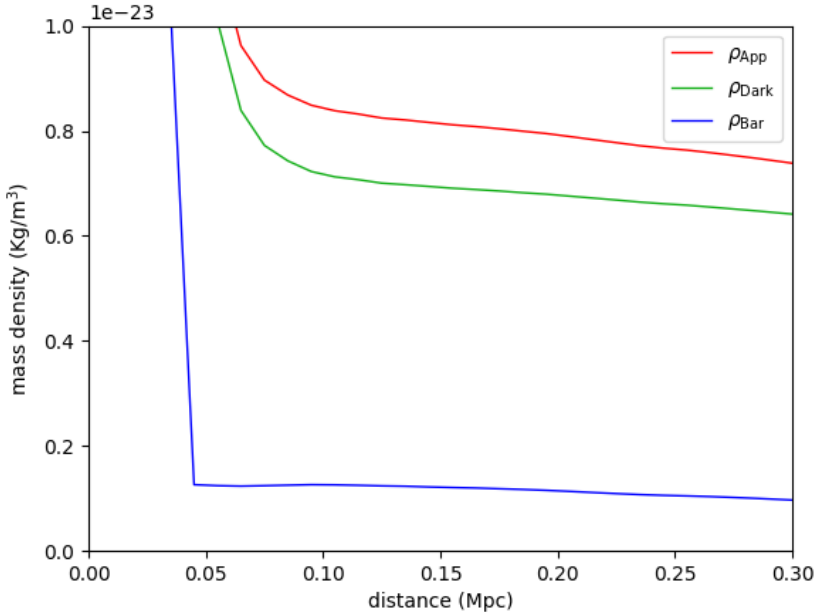

Figure 20: The average apparent, dark and baryonic mass density against the distance from a galaxy inside a cluster of 500 galaxies. All values are an average over 25 simulations of the average over all galaxies inside a single cluster. This figure is an in the y-direction zoomed in version of 18.

5.5. Projected matter distributions

5.5.1. Example galaxy

In figure 21 once more a false colour map of the baryonic mass density in a cluster of 50 galaxies is shown. However now it is not just the mass density of one slice of a cluster, but the surface mass density of the entire projected cluster. So all mass densities of the initial galaxy cluster have been integrated over the z-axis to get a surface mass density, in kg/m^2. In figure 22 the same is plotted but now for the apparent mass density. Note that the oscillating crosses coming out of the galaxies are artifacts of the Fourier transform. We already mentioned this when looking at the apparent mass density of the slices of a normal cluster.

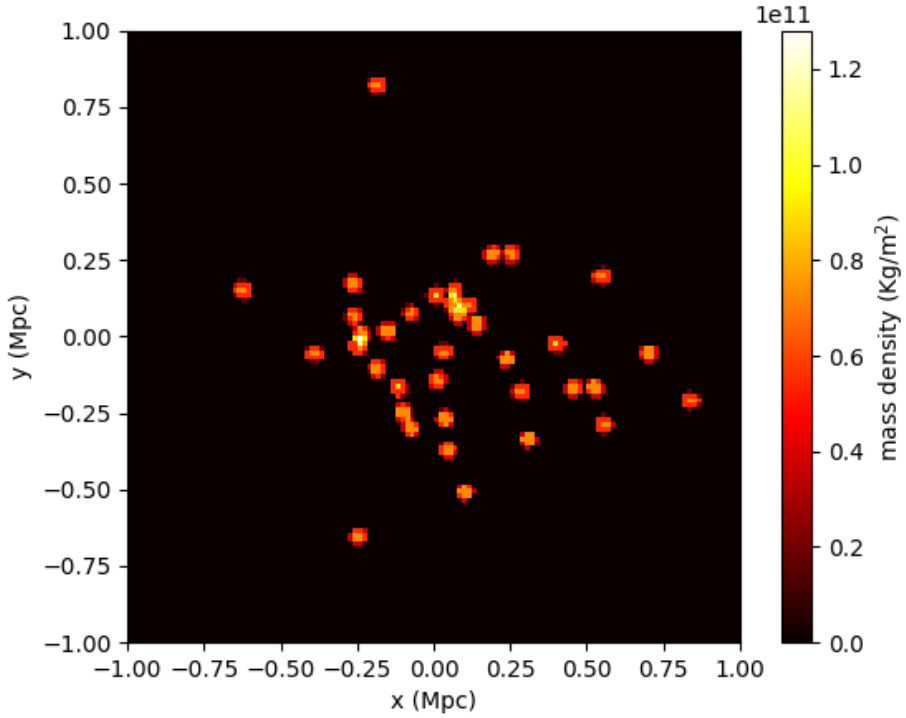

Figure 21: False colour map of the baryonic area mass density in a projected galaxy cluster with 50 galaxies plotted against the x and y location of the mass density.

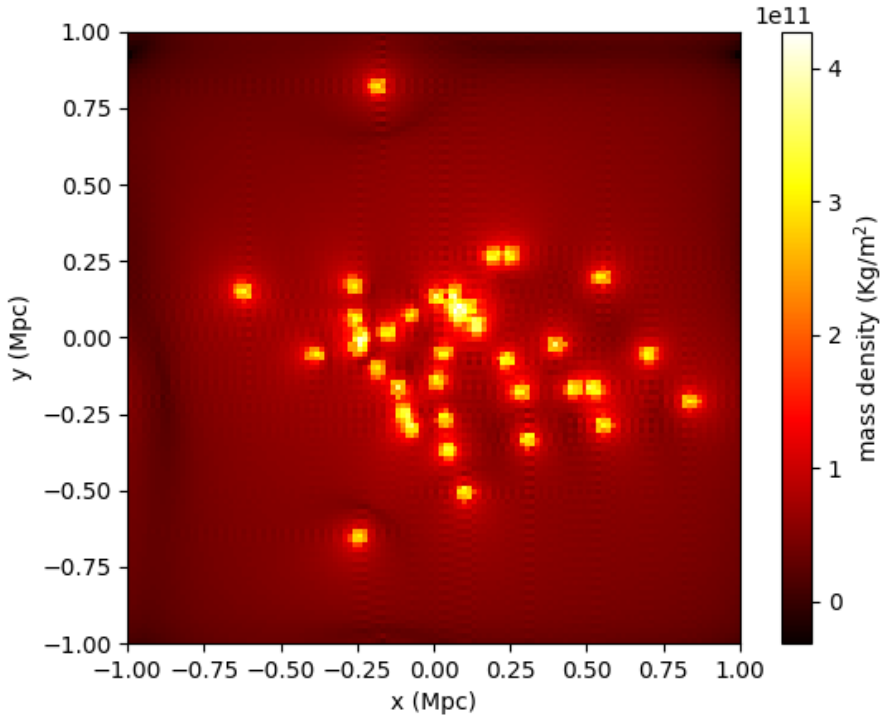

Figure 22: False colour map of the apparent area mass density in a projected galaxy cluster with 50 galaxies plotted against the x and y location of the mass density.

5.5.2. Mass in concentric circles around projected galaxies

Now we will look at the total apparent, dark and baryonic mass around the onto the xy-plane projected galaxies. We do this in a similar way to section 5.4.1, the only difference being that now everything happens in 2d instead of 3d. So instead of looking at the mass inside of concentric spheres we will calculate the mass inside concentric circles around the center of galaxies. We do this for the same 100 radii, so $r_0, r_1, ..., r_{100}$, where $r_n = n \cdot 0.0033$ Mpc. Then for each galaxy we calculate the total apparent mass M_{App}, dark mass M_{Dark} and baryonic mass M_{Bar}. Now we take the average over all galaxies in the cluster. This we do for all 25 simulations and then we also take the average over all clusters.

In figure 23 several plots of the average amount of M_{App}, M_{Dark} and M_{Bar} inside a circle with radius r against the radius r are shown. The two upper plots show the amount of apparent dark and baryonic matter for a cluster with 50 galaxies, were the plot in the upper right of figure 23 is a zoomed in version of the plot in the upper left. The same is true for the bottom plots, where the same is plotted for the average over 25 simulations of clusters with 500 galaxies. In contrast with the figures in section 5.4.1 we have now left out the individual values of all 25 simulations, to not overcrowd the figure.

In all plots the curves for apparent and dark matter are smoother and different phases are more difficult to distinguish when compared to the similar plots for the original, not projected, galaxy. This is probably a result of the fact that the clusters are located closer together, as they are projected onto the xy-plane. For the clusters with 50 galaxies the distinction between the linear part and the quadratic part of the plot is still visible.

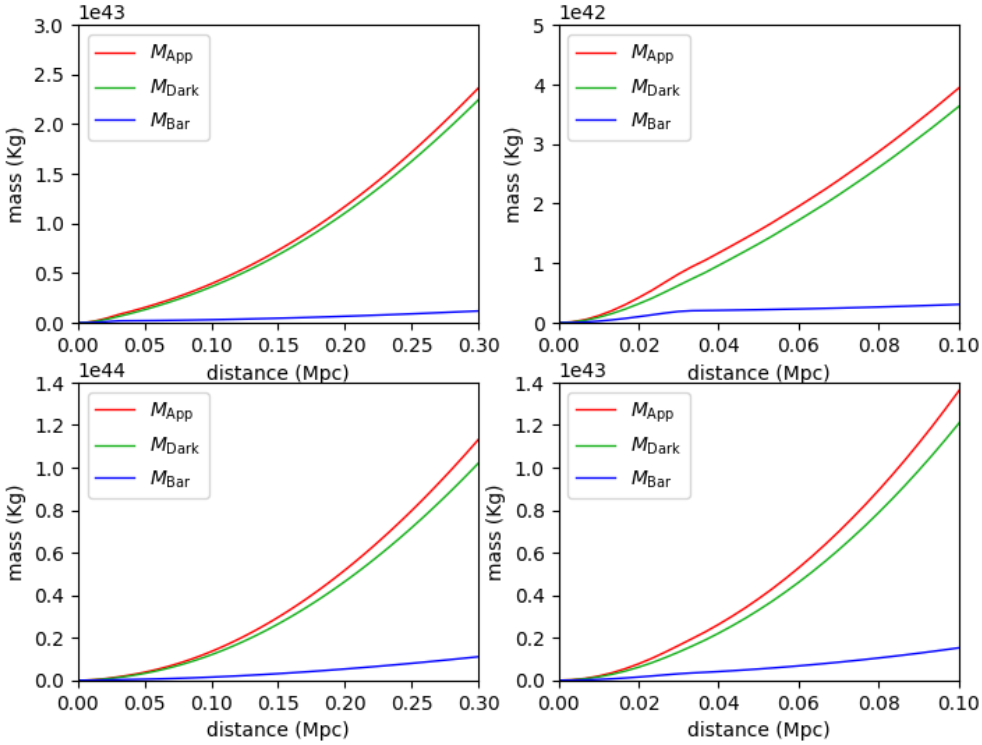

Figure 23: The average apparent, dark and baryonic matter inside a circle around the center of a galaxy is plotted four times against the radius of the circle. This average is taken over 25 simulations. The upper two plots are of clusters with 50 galaxies, where the right most plot is a zoomed in version of the leftmost one. The same is true for the bottom two plot, but now with cluster containing 500 galaxies.

5.5.3. Surface mass densities around projected galaxies

We again also look at how the average apparent, dark and baryonic surface mass densities, $\rho_{A,\text{App}}$, $\rho_{A,\text{Dark}}$ and $\rho_{A,\text{Bar}}$, relate to the distance to the center of a galaxy in our clusters. As we now have a projected cluster we will be looking at the surface mass densities instead of mass densities.We calculate this using the values we also used in our previous calculations about total matter distribution. We again take half as much radii as for the total matter distributions, so we have $r_0, r_1, ..., r_{50}$, where $r_n = n \cdot 0.0066$, Mpc. Our formula for calculating the average mass density between two radii also changes when we are looking at the 2d case. We now have that:

$$\rho_A\left(\frac{r_i + r_{i+1}}{2}\right) = \frac{(M_{i+1} - M_i)}{\pi\left(r_{i+1}^2 - r_i^2\right)} \tag{124}$$

In figures 24 and 25 the average mass density, averaged over all galaxies in one cluster and over all 25 simulations, are plotted against distance for the simulations with 50 and 500 galaxies respectively. We see that for the simulations with 50 galaxies the baryonic mass density $\rho_{A,\text{Bar}}$ is no longer a constant value but looks like the shape of a quarter of an ellipse. This is the result of projecting the mass of the spherical galaxy onto the 2d plane and is what we would expect

theoretically. If the resolution was infinitely high this would be a perfect quarter of an ellipse.

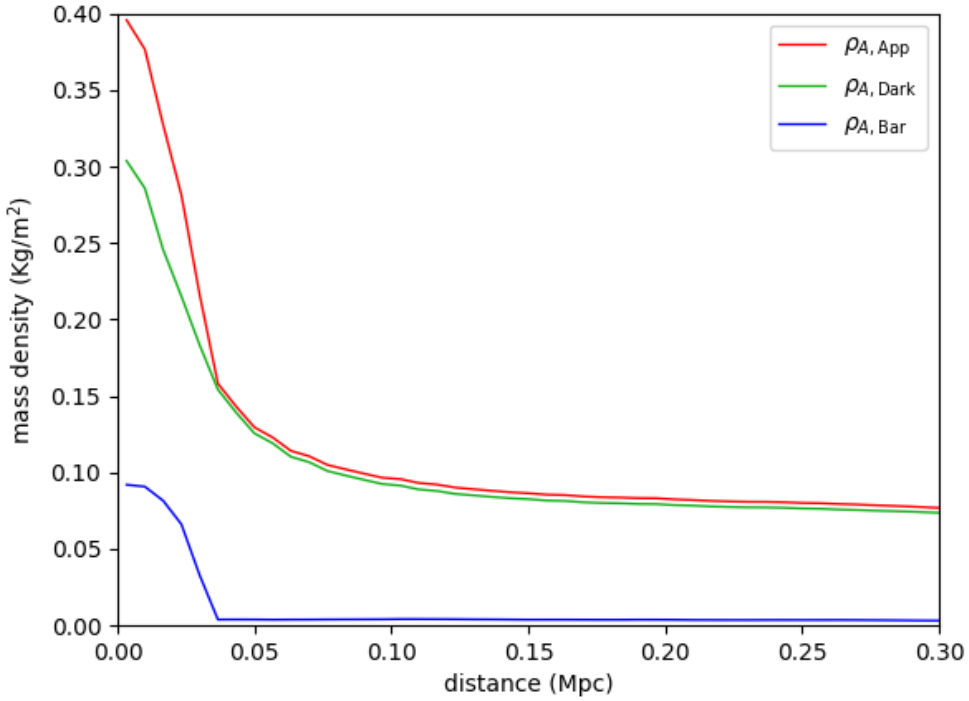

Figure 24: The average apparent, dark and baryonic mass per square meter against the distance from the center of a galaxy inside a cluster of 50 galaxies. All values are an average over 25 simulations of the average over all galaxies inside a single cluster.

We notice that the shape of $\rho_{A,\text{Dark}}$ inside the initial galaxy is quite different between the plot of the cluster with 50 galaxies and the one with 500 galaxies. Where the dark matter density increases very rapidly when nearing the center of the galaxy in the case of 50 galaxies per cluster, this increase is relatively much smaller in the case of 500 galaxies per cluster. For both cases we see that $\rho_{A,\text{Dark}}$ and $\rho_{A,\text{App}}$ are almost constant further away from the initial galaxy, but still decrease slightly. Again we notice that as a result of other galaxies being on average closer to the initial galaxy the apparent and dark mass densities stabilize sooner in the case of 500 galaxies per cluster.

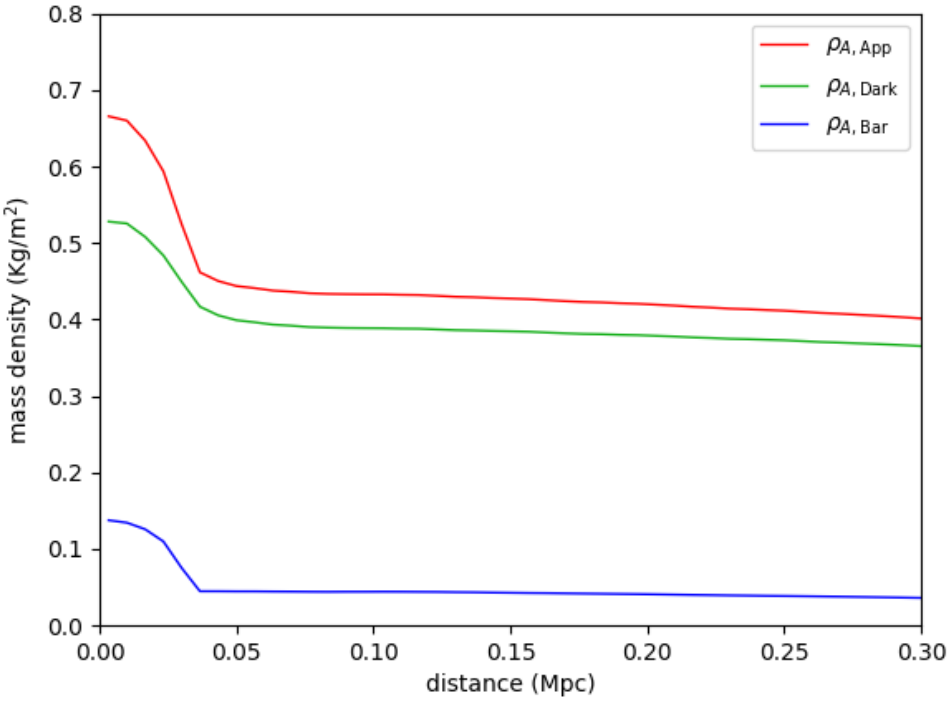

Figure 25: The average apparent, dark and baryonic mass per square meter against the distance from the center of a galaxy inside a cluster of 500 galaxies. All values are an average over 25 simulations of the average over all galaxies inside a single cluster.

6. Conclusion

To conclude we will summarize our findings and give some recommendations for future research. We have modeled galaxy clusters containing between 50 and 1000 galaxies with a baryonic mass of $3 \cdot 10^{41}$ Kg per galaxy distributed using an MOND isothermal spherically symmetric distribution function with $b = 0.4$ Mpc on a cubic region with dimensions 2 Mpc $\times$ 2 Mpc $\times$ 2 Mpc. We discretized this region into a grid of 256 $\times$ 256 $\times$ 256 points with a baryonic mass distribution. We modified the Poisson equation to make a Modified Newtonian Dynamics (MOND) equivalent function. We did this using the deep MOND regime of Modified Newtonian Dynamics, where we assume that the gravitational acceleration g is much smaller than Milgroms constant a_0 everywhere, $g << a_0$. Then to calculate the potential resulting from our mass distribution we used an iterative process to solve the MOND analogous Poisson equation. In this iterative process we made use of the standard Poisson equation, the discrete Fourier transform and the Helmholtz decomposition. All of these discrete calculations were made in Python.

We found that the maximum gravitational acceleration in a simulation of a galaxy with 50 galaxies was equal to $g_{\text{max},50} = 5.941 \cdot 10^{-11}$ m/s^2 $= 0.4575 \cdot a_0$. The gravitational acceleration is thus smaller then a_0 everywhere, but not much smaller, so the deep MOND regime is not a perfect assumption but still holds quite well. For the largest galaxy we looked at, we found $g_{\text{max},1000} = 1.002 \cdot 10^{-10}$ m/s^2 $= 0.8350 \cdot a_0$. Here we thus also do not have that the gravitational acceleration is much smaller then a_0 everywhere. However as it is still smaller then a_0 everywhere and much smaller in most places, we can still use the deep MOND regime without major complications.

Another thing we looked at was the ratio between the amount of apparent dark matter and baryonic matter, $\frac{M_{\text{Dark}}}{M_{\text{Bar}}}$, in a galaxy cluster. We studied this for clusters of varying amounts of galaxies, ranging from 50 to 1000 galaxies. We noticed that this ratio decreased when the amount of galaxies increased. This relation seemed to follow a relation of the form $\frac{M_{\text{Dark}}}{M_{\text{Bar}}} = a + \frac{b}{\sqrt{N}}$, where N is the amount of galaxies in a cluster. From a least squares fit we found the following values for these variables: $a = 0.8064 \pm 0.2383$ and $b = 101.9 \pm 4.3$. We must note that this relation should not be extrapolated for cluster of more than 1000 galaxies, as we would leave the deep MOND regime. A future study of this relation with full MOND would be very interesting.

When looking at the average apparent mass in a sphere with a certain radius around a galaxy we found three specific phases. We looked at clusters containing 50 and 500 galaxies and this was visible for both cases. In the first phase the average apparent mass increases seemingly quadratically while the radius is still smaller than the radius of the galaxy. Then, further away in the second phase, it increases linearly, being only influenced by the initial galaxy. We found that this linear increase is of the same order of magnitude as the theoretical value. Lastly, in the third phase, other galaxies start influencing the total mass and it increases quadratically again. As the chance of other galaxies located nearby is higher when more galaxies are present in the cluster, we see that the shift from a linear to a quadratic increase occurs earlier in this case.

We found that the average apparent mass density is the highest in the center of galaxies and decreases very quickly at a higher distance to galaxies. When the distance becomes high enough to reach neighbouring galaxies in the same cluster the average apparent mass density stabilizes and becomes almost constant, but still slightly decreases. This decrease occurs at a smaller distance when more galaxies are present in the cluster, as on average more galaxies are

located in the vicinity of the initial galaxy.

For clusters projected on a 2 dimensional plane we saw that the apparent dark matter area density was the highest inside galaxies. Outside of the galaxies this density reached an almost constant but still slightly decreasing value. This apparent area density distribution could be used for falsifying the MOND hypothesis in future research. Specifically an existing cluster could be reproduced in Python to compare the theoretical flattened apparent area density with observations of gravitational lensing.

Another interesting avenue of new research in this area could be taking a closer look at the locations of apparent mass as a result of the placements of galaxies in a cluster. We specifically took averages over all galaxies and over the φ and θ directions to look at the average apparent mass density distributions. By looking at the locations instead, more accurate predictions about the gravitational lensing events according to MOND could be made and possibly falsified.

References

[1] JG De Swart, Gianfranco Bertone, and Jeroen van Dongen. How dark matter came to matter. *Nature Astronomy*, 1(3):1–9, 2017.

[2] Gianfranco Bertone and Dan Hooper. History of dark matter. *Reviews of Modern Physics*, 90(4):045002, 2018.

[3] Kenneth C Freeman. On the disks of spiral and s0 galaxies. *The Astrophysical Journal*, 160:811–830, 1970.

[4] Vera C Rubin and W Kent Ford Jr. Rotation of the andromeda nebula from a spectroscopic survey of emission regions. *The Astrophysical Journal*, 159:379, 1970.

[5] KG Begeman, AH Broeils, and RH Sanders. Extended rotation curves of spiral galaxies: Dark haloes and modified dynamics. *Monthly Notices of the Royal Astronomical Society*, 249(3):523–537, 1991.

[6] R Brent Tully and J Richard Fisher. A new method of determining distances to galaxies. *Astronomy and Astrophysics*, 54:661–673, 1977.

[7] RH Sanders. A historical perspective on modified newtonian dynamics. *Canadian Journal of Physics*, 93(2):126–138, 2015.

[8] Mordehai Milgrom. A modification of the newtonian dynamics as a possible alternative to the hidden mass hypothesis. *The Astrophysical Journal*, 270:365–370, 1983.

[9] Jacob Bekenstein and Mordehai Milgrom. Does the missing mass problem signal the breakdown of newtonian gravity? *The Astrophysical Journal*, 286:7–14, 1984.

[10] Jacob D Bekenstein. Relativistic gravitation theory for the modified newtonian dynamics paradigm. *Physical Review D*, 70(8):083509, 2004.

[11] Constantinos Skordis and Tom Złośnik. New relativistic theory for modified newtonian dynamics. *Physical review letters*, 127(16):161302, 2021.

[12] Pedro VP Cunha and Carlos AR Herdeiro. Shadows and strong gravitational lensing: a brief review. *General Relativity and Gravitation*, 50(4):1–27, 2018.

[13] David J Griffiths. *Introduction to Electrodynamics*. Cambridge University Press, 2017.

[14] Benoit Famaey and James Binney. Modified newtonian dynamics in the milky way. *Monthly Notices of the Royal Astronomical Society*, 363(2):603–608, 2005.

Appendix

Below all code used for computations in this document is shown. The only code left out is the exact code used to make all images included. The code used to calculate each variable displayed in this document is included. First I will show the definitions of all constants and functions used in the code. Note that during this research often individual parts of this code were run and saved for further analysis, as doing all these computations takes quite a long time.

```
import numpy as np
import matplotlib.pyplot as plt
import time

#Constants

M = 1.5*10**11 #Solar Masses
Msol = 1.988*10**30 #Kg

rlyr = 105700   #lightyears
lyr = 9.4607*10**15 #m
mpc = 3.26e6 *lyr
r = rlyr*lyr
V = 4/3*np.pi*(r)**3
d = M*Msol/V    #kg/m^3
G = 6.67408*10**(-11) #m^3/kg/s^2
n_galaxies = 500
n_simulations = 25
nsteps = 256
nstepsc = nsteps*1j
length = 1*mpc

pi = np.pi
a0 = 1.2*10**(-10)
j = 1j
b= 0.5 *0.8* length

def phisphere(phi,r,M):
    n=0
    phinew = np.zeros(len(phi))
    for i in phi:
        if np.absolute(i) > r:
            phinew[n]= - M*G/np.absolute(i)
        else:
            phinew[n] = M*G*np.absolute(i)**2/(2*r**3)-3*M*G/(2*r)
        n=n+1
    return phinew

def Startcoordinates(n):
    c = np.zeros((n,3))
    for i in range(0,n):
        f = np.random.uniform(0,1)
        r = ((b**3*f**2+b**3*f+2*b**3*f**(3/2))/(1-f)**2)**(1/3)
        phi = 2*pi*np.random.uniform(0,1)
        q1 = np.random.uniform(0,1)
        theta = np.arccos(1-2*q1)
        c[i,0] = r*np.cos(phi)*np.sin(theta)
```

```
        c[i,1] = r*np.sin(phi)*np.sin(theta)
        c[i,2] = r*np.cos(theta)
    return c


def rhoarray(coordinates, length):
    array = np.zeros((nsteps,nsteps,nsteps))
    xyz = np.mgrid[-length+2*length/nsteps:length:nstepsc,-length+2*length/nsteps:length:nstepsc,-length+2*length/nsteps:length:nstepsc].reshape(3,-1).T
    for i in range(0,len(coordinates[:,0])):
        xyzloop = xyz - coordinates[i,:]
        squared = np.sum(xyzloop**2,axis = 1)
        squared2 = np.reshape(squared,(nsteps,nsteps,nsteps))
        rhoboolean = (squared2 <= r**2).astype(int)
        array = array + rhoboolean
    return array


def reshape3(Kmina):
    Kminxa = np.concatenate((Kmina[int(nsteps/2):nsteps,:,:], Kmina[0:int(nsteps/2),:,:]),axis=0)
    Kminxya = np.concatenate((Kminxa[:,int(nsteps/2):nsteps,:], Kminxa[:,0:int(nsteps/2),:]),axis=1)
    Kminxyza = np.concatenate((Kminxya[:,:,int(nsteps/2):nsteps], Kminxya[:,:,0:int(nsteps/2)]),axis=2)
    return Kminxyza


def fiteration(f0x,f0y,f0z):
    f0tildex,f0tildey,f0tildez = np.fft.fftn(f0x),np.fft.fftn(f0y),np.fft.fftn(f0z)

    innerproduct = (kx*f0tildex+ky*f0tildey+kz*f0tildez)*Kmin
    phinew = np.fft.ifftn(j*innerproduct)
    f1tildex = kx*innerproduct
    f1tildey = ky*innerproduct
    f1tildez = kz*innerproduct
    f1x,f1y,f1z = np.fft.ifftn(f1tildex),np.fft.ifftn(f1tildey),np.fft.ifftn(f1tildez)
    return f1x,f1y,f1z,phinew


def Biteration(f0x,f0y,f0z):
    fsquared2 = (f0x)**2+(f0y)**2+(f0z)**2
    B1x = 1/a0*np.sqrt(fsquared2)*f0x-gx
    B1y = 1/a0*np.sqrt(fsquared2)*f0y-gy
    B1z = 1/a0*np.sqrt(fsquared2)*f0z-gz
    B1tildex,B1tildey,B1tildez = np.fft.fftn(B1x), np.fft.fftn(B1y), np.fft.fftn(B1z)

    innerproduct = (kx*B1tildex+ky*B1tildey+kz*B1tildez)*Kmin
    B2tildex = B1tildex-kx*innerproduct
    B2tildey = B1tildey-ky*innerproduct
    B2tildez = B1tildez-kz*innerproduct
```

```
    B2x,B2y,B2z = np.fft.ifftn(B2tildex),np.fft.ifftn(B2tildey),np.fft.ifftn(B2tildez)
    gBsquared2 = (gx+B2x)**2+(gy+B2y)**2+(gz+B2z)**2
    f2x,f2y,f2z =  np.sqrt(a0/(np.sqrt(gBsquared2)))*(gx+B2x),np.sqrt(a0/(np.sqrt(gBsquared2)))*(gy+B2y),np.sqrt(a0/(np.sqrt(gBsquared2)))*(gz+B2z)
    return f2x,f2y,f2z,B2x,B2y,B2z

def Monditerations(f0xmond,f0mondy,f0mondz,n):
    i=0
    while i<n:
        f1x,f1y,f1z,phinew = fiteration(f0xmond,f0mondy,f0mondz)
        f0xmond,f0mondy,f0mondz,B0x,B0y,B0z = Biteration(f1x.astype('float64'),f1y.astype('float64'),f1z.astype('float64'))
        i+=1
    return f0xmond,f0mondy,f0mondz,B0x,B0y,B0z,phinew

def densitycalculation(phiend):
    phitilde = np.fft.fftn(phiend)
    rhotilde = -Kminxyz*phitilde/(4*np.pi*G)
    rhonew = np.fft.ifftn(rhotilde).astype('float64')
    return rhonew

def mass_inside_radius(coordinates,rho,rho_app,r,n):
    total_mass = np.zeros(n+1)
    total_mass_dark = np.zeros(n+1)
    total_mass_visible = np.zeros(n+1)

    xyz = np.mgrid[-length+2*length/nsteps:length:nstepsc,-length+2*length/nsteps:length:nstepsc,-length+2*length/nsteps:length:nstepsc].reshape(3,-1).T
    for i in range(0,len(coordinates[:,0])):
        xyzloop = xyz - coordinates[i,:]
        squared = np.sum(xyzloop**2,axis = 1)
        squared2 = np.reshape(squared,(nsteps,nsteps,nsteps))
        for j in range(n):
            inside_radius_rho = rho[np.where(squared2 <= r[j+1]**2)]
            inside_radius_rho_app = rho_app[np.where(squared2 <= r[j+1] ** 2)]
            mass_visible = sum(inside_radius_rho) * (2*length / nsteps) ** 3
            mass = sum(inside_radius_rho_app) * (2*length / nsteps) ** 3
            mass_dark = mass-mass_visible
            total_mass[j+1] += mass
            total_mass_dark[j+1] += mass_dark
            total_mass_visible[j+1] += mass_visible
    avg_mass = total_mass/len(coordinates[:,0])
    avg_mass_dark = total_mass_dark/len(coordinates[:,0])
    avg_mass_visible = total_mass_visible/len(coordinates[:,0])

    return avg_mass,avg_mass_dark,avg_mass_visible

def mass_ratio():
    total_ratio = 0

```

```
    for simulation in range(n_simulations):
        a = 0
        for i in range(int(nsteps / 4), int(3 * nsteps / 4)):
            for k in range(int(nsteps / 4), int(3 * nsteps / 4)):
                for l in range(int(nsteps / 4), int(3 * nsteps / 4)):
                    a = a + rho_list[simulation][i, k, l] * (length / nsteps) ** 3

        a2 = 0
        for i in range(int(nsteps / 4), int(3 * nsteps / 4)):
            for k in range(int(nsteps / 4), int(3 * nsteps / 4)):
                for l in range(int(nsteps / 4), int(3 * nsteps / 4)):
                    a2 = a2 + rho_app_list[simulation][i, k, l] * (length / nsteps) ** 3
        total_ratio += a2 / a
    average_ratio = total_ratio / n_simulations
    return average_ratio

def projected_mass_inside_radius(coordinates,rho,rho_app,r,n):
    total_mass = np.zeros(n+1)
    total_mass_dark = np.zeros(n+1)
    total_mass_visible = np.zeros(n+1)
    rho_squeezed = np.sum(rho,axis=0)
    rho_app_squeezed = np.sum(rho_app, axis=0)
    xyz = np.mgrid[-length+2*length/nsteps:length:nstepsc,-length+2*length/nsteps:length:nstepsc].reshape(2,-1).T
    for i in range(0,len(coordinates[:,0])):
        xyzloop = xyz - coordinates[i,1:]
        squared = np.sum(xyzloop**2,axis = 1)
        squared2 = np.reshape(squared,(nsteps,nsteps))
        for j in range(n):
            inside_radius_rho = rho_squeezed[np.where(squared2 <= r[j+1]**2)]
            inside_radius_rho_app = rho_app_squeezed[np.where(squared2 <= r[j+1] ** 2)]
            mass_visible = sum(inside_radius_rho) * (length / nsteps) ** 3
            mass = sum(inside_radius_rho_app) * (length / nsteps) ** 3
            mass_dark = mass-mass_visible
            total_mass[j+1] += mass
            total_mass_dark[j+1] += mass_dark
            total_mass_visible[j+1] += mass_visible
    avg_mass = total_mass/len(coordinates[:,0])
    avg_mass_dark = total_mass_dark/len(coordinates[:,0])
    avg_mass_visible = total_mass_visible/len(coordinates[:,0])

    return avg_mass,avg_mass_dark,avg_mass_visible
```

Below the main code in which all individual functions are called is displayed.

```

coords = Startcoordinates(n_galaxies)
rhoboolean = rhoarray(coords,length)
rho = d*rhoboolean

rhotilde = np.fft.fftn(rho)

kvector = np.mgrid[-pi*nsteps/(2*length):pi*nsteps/(2*length)-pi/length:
```

```
    nstepsc, -pi*nsteps/(2*length):pi*nsteps/(2*length)-pi/length:nstepsc,-
    pi*nsteps/(2*length):pi*nsteps/(2*length)-pi/length:nstepsc]
kx = reshape3(kvector[0])
ky = reshape3(kvector[1])
kz = reshape3(kvector[2])

K = np.sum((kvector.reshape(3,-1).T)**2,axis = 1)

Kmin = K
Kmin = np.reshape(Kmin,(nsteps,nsteps,nsteps))
Kminxyz = reshape3(Kmin)
Kmin = 1/Kminxyz
Kmin[0,0,0] = 0
phitilde = - 4 * np.pi * G * rhotilde*Kmin

phi = np.fft.ifftn(phitilde).astype('float64')

gx_tilde = -j*np.multiply(kx,phitilde)
gy_tilde = -j*np.multiply(ky,phitilde)
gz_tilde = -j*np.multiply(kz,phitilde)

gx = np.fft.ifftn(gx_tilde)
gy = np.fft.ifftn(gy_tilde)
gz = np.fft.ifftn(gz_tilde)

g = np.sum([gx**2,gy**2,gz**2],axis=0)**0.5
g_inv = 1/g

for i in range(0,nsteps):
    for k in range(0,nsteps):
        for l in range(0,nsteps):
            if g[i,k,l]==0:
                g_inv[i,k,l] = 0


f0x,f0y,f0z = np.sqrt(a0*np.sqrt(g_inv))*gx,np.sqrt(a0*np.sqrt(g_inv))*gy,
    np.sqrt(a0*np.sqrt(g_inv))*gz
fendx,fendy,fendz,Bendx,Bendy,Bendz,phiend = Monditerations(f0x,f0y,f0z,5)



rho_app= densitycalculation(phiend)

ratio = mass_ratio()

max_radius =length / 3
n = 100
r = np.linspace(0, max_radius, n + 1)

avg_mass, avg_mass_dark, avg_mass_visible = mass_inside_radius(coords, rho,
     rho_app,r,n)

projected_avg_mass, projected_avg_mass_dark, projected_avg_mass_visible =
    projected_mass_inside_radius(coords, rho, rho_app,r,n)
```